NTNU – Trondheim
Norwegian University of
Science and Technology

UPSCALING OF WELL LOG DATA FOR A TRANSVERSE ISOTROPIC EFFECTIVE MEDIUM

Eric Ameyaw Debrah

Petroleum Geosciences
Submission date: June 2013
Supervisor: Alexey Stovas, IPT

Norwegian University of Science and Technology
Department of Petroleum Engineering and Applied Geophysics

UPSCALING OF WELL LOG DATA FOR A TRANSVERSE ISOTROPIC EFFECTIVE MEDIUM

A Thesis

by

ERIC DEBRAH AMEYAW

Submitted to the office of Graduate studies of

Norwegian University of Science and Technology

in partial fulfillment of the requirements for the degree of

Master of Science (Petroleum Geophysics)

June 2013

Abstract

We develop two methods to determine; (1) net to gross and hydrocarbon saturation in a mixture of sand and shale. (2) effective properties versus tilt in sand. Backus (1962) and Schoenberg and Muir (1989) averaging are used for the horizontally layered transversely isotropic medium with vertical symmetry axis (VTI), horizontal symmetry axis (HTI) and tilted symmetry axis (TTI) test respectively. A mixture of two points representing sand and shale are picked from Intrabasalt 2 formation (North Sea data) and the effective properties and anisotropic parameters (epsilon, delta and gamma) are computed using matlab algorithm. The modeling results for the VTI, HTI and TTI show that P- wave velocity (v_p) increases with increasing net to gross and S- wave velocity (v_s) decreases with increasing net to gross. The anisotropic parameters decrease with increasing net to gross. In the second part, the whole Intrabasalt 2 formation is considered as sand in a tilt form. The modeling results show that P- wave velocity and S- wave velocity increase with increasing tilt angle in sand and the anisotropic parameters of the tilt sand decrease with increasing tilt angle with the exception of anisotropic parameter delta which increases with tilt angle up to 30° and then decreases with increasing tilt angle up to 90°

Acknowledgements

I thank the Almighty God for his unchanging favor and absolute sustenance in my research work. I would like to express my deepest appreciation to my supervisor Professor Alexey Stovas for his guidance, encouragement and support throughout the computation and the write up. He really introduced me into the rock physics world and taught me with much patience. May God richly bless him and his family.

I would like to thank my classmates who spent their invaluable time to go through the thesis. Most especially to Juan Carlos Flores, Yan and Eze Celestine.

I am very grateful to my best female friends and classmates for their pieces of advice. They are Alexandria and Paola, from Norway and Venezuela respectively.

My thanks to all NTNU students for their selfless and dedication towards sharing of ideas. I am very enthused.

I am greatly indebted to my mother, Faustina Animah and my twin sister Akua Serwaa Debrah for their prayers and moral support. I owe them much gratitude. May the good God continue to shower his blessings upon them.

Table of Contents

CHAPTER ONE

1.0 Introduction

1.1 Motivation and Objective

Transverse isotropy (TI) results in more accurate models of wave propagation than the ones based on isotropy assumption for characterizing seismic data. Seismic analysis requires calibration of seismic data with well logs. Well log data need to be upscaled to seismic frequency, and the upscaling is normally done with the Backus averaging (Backus 1962). Backus averaging is a harmonic mean of combination of elastic moduli computed from well log data for a desired depth thickness. Anisotropy caused by fine layering is often considered responsible for the differences between velocities achieved in sonic log and seismic experiments. To understand the link between velocities obtained in upscaling is crucial, especially, in the current era of most wells being highly deviated. The goal of the upscaling of heterogeneous media is to simplify the earth model without changing the overall seismic wavefield during wave propagation (Gold et al., 2000).

Vertical sonic velocities can be upscaled according to Backus (1962) to deduce interval velocities for seismic frequencies. For a medium with two constituents, such as shale and sand, the anisotropic parameters of both layers should be known to predict the properties of the effective compound (Backus, 1962). Complete specification of a transverse isotropy medium requires defining seven parameters at every subsurface location, namely five stiffnesses and two angles specifying the symmetry axis orientation. Modeling the subsurface by transverse isotropy with a vertical axis of symmetry is normally adequate for inverting or imaging surface seismic data. There is a growing interest in exploration of shale reservoir, and many of the shale reservoirs are fractured (Younes et al 2010, Gaiser et al 2011). Fractures and faults are common in the subsurface of the Earth's crust and they control much of the mechanical strength and transport properties of the solid structure. Fractures and fracture systems are also crucial for hydrocarbon exploration. In particular, shales overlay over 70% of

hydrocarbon exploration targets and are known to have transversely isotropic properties due to microstructure associated with the layering of fine clay platelets (Sayers, 1994). Several theories of modeling wave propagation in cracked rocks have been developed. However, a few of them can model large fractures and fluid flow in fractured rock. In this write up, I used the Backus (1962) averaging and Schoenberg and Muir (1989) method for the upscaling. I considered transverse isotropy with vertical symmetry axis (VTI), horizontal symmetry axis (HTI) and tilted symmetry axis (TTI).

The main objectives of the thesis are;

1. To discriminate between sand and shale using secondary properties such as acoustic impedance and v_p / v_s ratio.

2. To determine the effect on effective properties versus net to gross (N/G).

3. To determine the effect on effective properties versus tilt angle in sand layers.

1.2 Background for well log Data

The aim of the Geophysicists is to produce the reliable seismic data from experiments such as well logging. Generally, boreholes are drilled to the depth to be examined, and logging instruments measure properties of the subsurface inside boreholes with increasing depth. We use the well log data to analyze physical properties of the rocks and to obtain corresponding petrophysical properties such as porosity, permeability, water saturation etc. For the purpose of this research, one well log data from the North Sea is used. The data contains v_p, v_s, density, and anisotropic parameters epsilon, delta and gamma. Vp-Vs ratio and acoustic impedance are computed from the data and subsequently used for lithology discrimination.

1.3 Upscaling Problem of Well log Data

“Upscaling” in this context implies the theoretical prediction of the effective elastic properties at seismic frequency using well log data. Heterogeneities in the earth’s subsurface result in variations in the elastic constants in rocks. The inhomogeneous properties cause problems in seismic interpretation because of the complex link between heterogeneity and wave amplitudes. Moreover, randomly varying rock component such as cracks, micro-cracks and saturation make it impossible to solve the inverse problem from the measured data. To get reliable results from data processing, the upscaling method relating the small scale to the large scale has been paramount for the Geophysicists over the years. Also, recent advances of precise and fast computing technology have increased the demand for quantitative predictions and higher resolutions in the earth model from effective upscaling methods such as Backus (1962).

1.4 Fundamentals

With respect to wave propagation, Stovas and Arntsen (2006) mentioned that the wave propagation velocity strongly depends on the ratio (λ/d) of the dominant wavelength to the typical layer thickness. When the wavelength is large comparing with the layer thickness, the wave velocity can be given by an average of the properties in individual layers (Backus, 1962), and waves behave as if propagating in an effective isotropic homogeneous medium even if the medium is anisotropic. On the other hand, when the wavelength is small comparing with the layer thickness, the waves behave in line with the ray theory because of high frequency approximation.

Experimental research depicts that sonic log data include a large fluctuation in P-wave and S-wave velocities, and this fluctuation decreases at the lower frequencies of the seismic data.

Therefore, in a logical sense, Backus averaging means the replacement of heterogeneous volume with a homogeneous volume containing effectively equivalent elastic constants. It is also a process, whereby a stack of thin layers is averaged until it

is approximated by the properties of a single thick layer. From this analogy, it is reasonable to replace many thin layers with one thick layer. With a lack of more easily detected reservoirs, recently found reservoirs have geologically more heterogeneous structures. To identify these, we need to consider all heterogeneous effects on the small scale data, but it is very inefficient to resolve the heterogeneity from numerous numerical simulations because of the excessive computing time. Therefore the goal of the Geophysicists is to make precise, cost saving and timely decisions in all kinds of data analysis.

1.5 Previous works

In finely layered media, the way and manner in which the wave propagates has been the main interest of Geophysicists. Anderson (1961), Thomson (1950) and Helbig (1958) examined homogeneous anisotropic multilayered cases. Thomson (1950) gave a formal solution for waves of arbitrary wavelength in a medium with homogeneous isotropic layers, and found the displacement and vertical stresses at any interface. Helbig (1958) represented formulae for five elastic coefficients as averages and generalized them to a multilayered case, yet he did not consider anisotropic layers. Afterwards, Anderson (1961) applied the formulae to anisotropic layered media.

In spite of the efforts made by these people, I can confirm that upscaling process such as transverse isotropy using well log examples have been developed by many other people.

A practical basis of the averaging method was made by Backus (1962). He showed that waves behave as if going through a homogeneous and transversely isotropic medium in case that the waves have a large enough wavelength comparing with a layer thickness (Backus, 1962). The Backus approach is advantageous for two main reasons. First, it gives simple expressions for elastic constants as averages of elastic moduli. Secondly, it can be applied to non-periodic layered media with more than two constituents, which may be transversely isotropic themselves. It has also been extended to the case where

the constituents themselves are anisotropic (Schoenberg and Muir, 1989). It is also well understood that layered media are both dispersive and anisotropic to elastic waves. These characteristics depend on the dimensions relative to the wavelengths, the proportions, and the intrinsic physical properties of the constitutive materials.

At ‘long’ wavelengths a layered structure will behave as one ‘effective’ medium. In contrast, at sufficiently ‘short’ wavelengths each of the individual components of the structure will influence the transmitted waves according to optical ray theory. The elastic wave velocity of such a medium can be highly dispersive. In spite of these, nearly all of seismology assumes the elastic energy is transmitted according to ray theory. This could lead to some inconsistencies, the perennial time mismatch between synthetic seismograms, calculated on the basis of ray theory through thin layers defined by the sonic log spatial sampling, and events within reflection profiles being one such example of this phenomena (e.g., Rio et al ., 1997; IMHOF, 2004). However, such effects need to be considered when core based studies (~1 MHz) are integrated with log (~20 kHz) and seismic (~ 100 Hz) data. Further, it is cumbersome for us to know what the true structural scaling is within the Earth. This may add additional uncertainty to our interpretations of an observed seismic velocity. Having a better understanding of how such dispersion influences seismic velocity and anisotropy is important to the understanding of observations at many scales.

1.6 Scope of the Thesis

The major content of this thesis consists of five chapters characterized by upscaling technique. In chapter one, motivation and objectives are introduced briefly, and basic concepts of upscaling are highlighted. Chapter two explains the concept and theoretical background of seismic anisotropy, effective medium, Backus (1962) averaging, Schoenberg and Muir (1989) theory etc.

Chapter three also explains the method employed for the thesis, thus Backus (1962) averaging method and Schoenberg and Muir (1989) method. Discrimination between

sand and shale, selection of sand and shale and their analysis using well log data containing effective properties v_p, v_s, density and anisotropic parameters epsilon, delta and gamma are also discussed. Chapter four explains the meaning of the models obtained and chapter five finally, summarizes the whole write up.

CHAPTER TWO

2.0 Theoretical Background

2.1 Rock Physics and seismology

There is a growing interest in exploration of shale reservoirs, and many of the shale reservoirs are fractured (Younes et al 2010, Gaiser et al 2011). Fracturing of rock can induce lower symmetry seismic anisotropy. Seismology is one of the most important geophysical fields to find and monitor petroleum reservoirs by seismically imaging the earth's reflectivity distribution. The exploration Geophysicists perform seismic experiments similar to that shown in figure 1 and 2. To interprete these reflection data into knowledge of geological structures in which the waves have travelled, one needs a physical model that describes how waves act in different media. Deformations of rocks due to seismic waves are normally assumed to be linearly elastic. Because wave propagation depends upon the elastic properties of the rocks, the concept of elasticity is explained in this write up. A material is defined as continuous if it contains no empty spaces and its properties can be described by spatially continuous functions. The size and shape of a solid body can be changed by applying forces to the external surface of a body. These external forces are opposed by internal forces which resist changes in size and shape. A fluid resists changes in size (volume) but not changes in shape. The property of resisting changes in size or shape and returning to the undeformed condition when the external forces are removed is known as elasticity. Many substances including rocks can be considered perfectly elastic because most rocks recover completely after being deformed. Rock formations built up of different rock types are separated by interfaces where the physical properties are discontinuous. The theory of elasticity relates the forces that are applied to the external surface of a body to the resulting changes in size and shape. The relations between the applied forces and the deformations are most conveniently expressed in terms of the concepts of stress and strain. Strain is a change in shape and is proportional to the stress that produces it. The constant of proportionality is called elastic constant. Most seismic theory assumes that media are isotropic, that is their properties are the same irrespective of the direction of

measurement. Anisotropy of several types has been observed. The most important with regard to the thesis is transverse isotropy, simply because of layering and fracturing.

The figures below show what happens to seismic body waves as they travel in the earth.

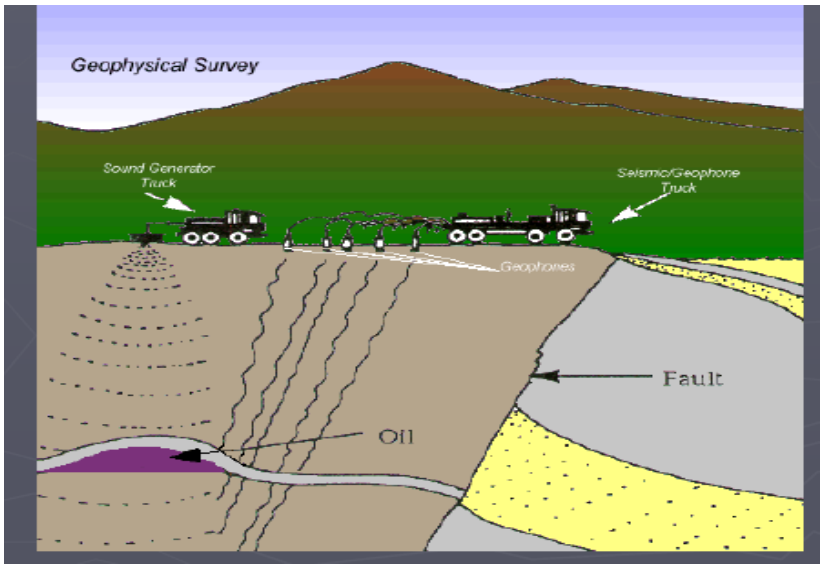

Figure 1. Seismic waves travelling through the earth (onshore seismic survey).

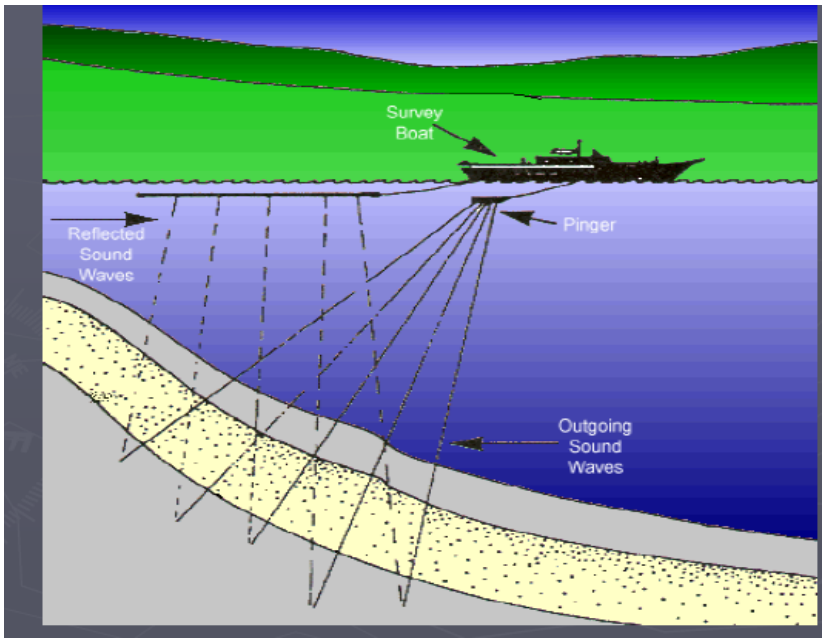

Figure 2. Seismic waves travelling through the earth (offshore surveys).

2.2 Hooke's law

Knowing the relationship between stress and strain helps us to calculate the strains when the stresses are applied. When several stresses exist, each produces strains independently of the others; hence, the total strain is the sum of the strains produced by the individual stresses and vice versa. In general, Hooke's law leads to complicated relation. Stress and strain can both be regarded as second-order (3x3) matrices so that the Hooke's law proportionality relating them is a fourth-order tensor. Many of the physical quantities in this write up are described in terms of tensors. The Hooke's law is a statement that the stress is proportional to the gradient of the deformation occurring in the material. We consider that the continuum material is a linear elastic material, so we introduce the generalized Hooke's law in Cartesian coordinates

$$\boldsymbol{\sigma}_{ij} = \mathbf{C}_{ijkl}\boldsymbol{\varepsilon}_{kl}\,, \tag{1}$$

where $\boldsymbol{\sigma}_{ij}$ is the stress component, $\mathbf{C}_{ijkl}$ is the stiffness tensor and $\boldsymbol{\varepsilon}_{kl}$ is the strain component.

These equations assume that a linear relationship exists between the components of stress and strain tensor. They relate stress and strain, because they depend on the material behavior, whether it being an elastic or plastic solid or a viscous fluid. The equations are applicable for materials exhibiting small deformations subjected to external forces. The 81 constants C_{ijkl} are called the elastic stiffness of the material and are the components of a Cartesian tensor of the fourth order. In terms of anisotropy, the material is represented by the fact that the components of C_{ijkl} are in general different for different choices of coordinate axes. If the body is homogeneous, that is, the mechanical properties are the same for every particle of the body, and then C_{ijkl} are constants. If a tensor has certain symmetry, the representation only needs as many components as the number of independent components in the tensor. Therefore we convert the $3\times3\times3\times3$tensor $\mathbf{C}_{ijkl}$ to the 6×6matrix $\mathbf{C}_{\alpha\beta}$using the mapping:

$$ij = ji = 11 \;\; 22 \;\; 33 \;\; 23 \;\; 13 \;\; 12$$

$$\downarrow \;\; \downarrow \;\; \downarrow \;\; \downarrow \;\; \downarrow \;\; \downarrow \;\; \downarrow$$

$$\alpha = 1 \;\; 2 \;\; 3 \;\; 4 \;\; 5 \;\; 6$$

2.3 Symmetries

In the “worst case” the stiffness tensor has 21 independent elements giving us “triclinic “ symmetry. Equation (2) is an example of the “worst case”.

$$[C] \equiv \begin{pmatrix} C_{11} & C_{12} & C_{13} & C_{14} & C_{15} & C_{16} \\ C_{12} & C_{22} & C_{23} & C_{24} & C_{25} & C_{26} \\ C_{13} & C_{23} & C_{33} & C_{34} & C_{35} & C_{36} \\ C_{14} & C_{24} & C_{34} & C_{44} & C_{45} & C_{46} \\ C_{15} & C_{25} & C_{35} & C_{45} & C_{55} & C_{56} \\ C_{16} & C_{26} & C_{36} & C_{46} & C_{56} & C_{66} \end{pmatrix}. \qquad (2)$$

If the material has a particular symmetry, the number of independent components is reduced.

2.4. Seismic Anisotropy

In recent years, seismic anisotropy has become a challenging topic in the oil and gas industry. The anisotropic nature of sedimentary basins containing oil and gas reservoirs can lead to higher micro-seismic event location errors if the velocity models used for the reservoir do not accurately account for anisotropy.

Seismic anisotropy is defined as ‘the dependence of seismic velocity upon angle’ (Thomsen, 2002). It is also defined as ‘a variation of a physical property depending on the direction in which it is measured’ (Sherriff, 2002).

Anisotropy is a very useful attribute for the detection and characterization of aligned fracture sets in reservoirs (Alan et al, 2012). There are several mechanics which may

contribute to the anisotropy of sedimentary rocks. We have fractures, microcracks, cracks etc. For example there could be anisotropy related to the rock fabric, such as the preferred alignment of intrinsically anisotropic minerals (eg. Vernik and Nur, 1992; Valcke et al., 2006; Kendall et al., 2007), or the periodic layering of contrasting lithologies (eg. Backus, 1962). The idea of distinguishing between the different sources of anisotropy can be of good help by making estimates about their respective symmetry and orientation. For example, the fabric of sedimentary rocks is typically aligned horizontally, which produces an anisotropy system with a vertical axis of symmetry (VTI). Fig 3 is a typical example. Fractures and cracks within a medium are normally vertical or dipping, producing horizontal transverse isotropy (HTI). The lack of axisymmetry in rock may be related to a lack of axisymmetry in the stress field. Crampin (1985) argued that stress anisotropy causes rock anisotropy by creating aligned microcracks. Whether this is so or not is very cumbersome to establish, because drilling and coring distort the stress field and close cracks that might have existed in situ. A set of parallel fractures orthogonal to bedding planes for example vertical fractures and horizontal bedding gives orthorhombic symmetry in the long wavelength limit (Shoenberg, 1986). When a single set of parallel fractures is neither perpendicular nor parallel to bedding, the equivalent medium is monoclinic (Shoenberg, 1985). These are encountered in the earth and can be manipulated using matrix methods.

Backus (1962) also showed that a region composed of several layers is equivalent in the long wavelength limit to a homogeneous, transversely isotropic medium and that the properties of this equivalent medium can be derived using appropriate techniques. The figures below show how VTI anisotropy characterizes horizontal layering and HTI anisotropy characterizes vertical fracturing.

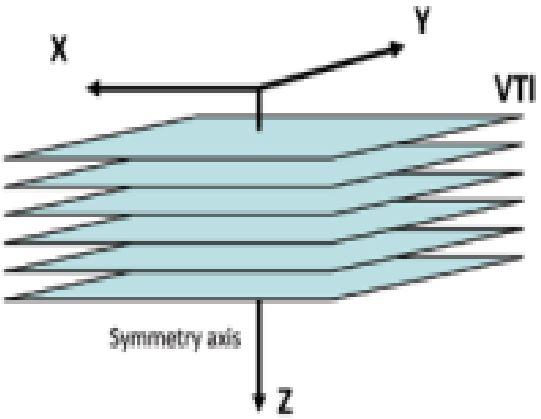

Figure 3. VTI anisotropy characterising horizontal layering.

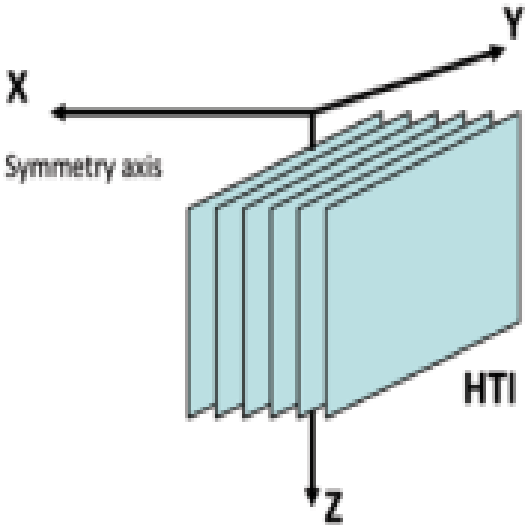

Figure 4. HTI anisotropy characterising vertical fracturing.

The most popular anisotropic model is TI anisotropy.

2.4.1. Isotropy

Isotropic symmetry is the simplest type of symmetry which helps us to understand wave propagation in the earth. In a homogeneous region, where the seismic waves propagate equally fast in all directions, the stiffness is given as;

$$\begin{pmatrix} C_{11} & (C_{11}-2C_{66}) & C_{13} & 0 & 0 & 0 \\ C_{11}-2C_{66} & C_{11} & C_{13} & 0 & 0 & 0 \\ C_{13} & C_{13} & C_{33} & 0 & 0 & 0 \\ 0 & 0 & 0 & C_{44} & 0 & 0 \\ 0 & 0 & 0 & 0 & C_{44} & 0 \\ 0 & 0 & 0 & 0 & 0 & C_{66} \end{pmatrix}. \quad (3)$$

This symmetry is called 'polar' symmetry, simply because it has a single pole of rotational symmetry. It is the symmetry of the horizontal thin-bed-sequence or of horizontal massive shale.

The wave velocities in an isotropic medium are independent of propagation direction and they are given by

$$V_p = \sqrt{\frac{C_{33}}{\rho}} \quad , \quad (4)$$

$$V_s = \sqrt{\frac{C_{44}}{\rho}} \quad . \quad (5)$$

We normally use the isotropic properties for reservoir modeling and simulation.

2.4.2 Transverse Isotropy

Transverse isotropy is another anisotropic model of practical importance. They are materials where the physical parameters are isotropic along horizons. It has a unique symmetry axis around which rotations do not utter the physical properties. The figure below shows the plane of transverse isotropy.

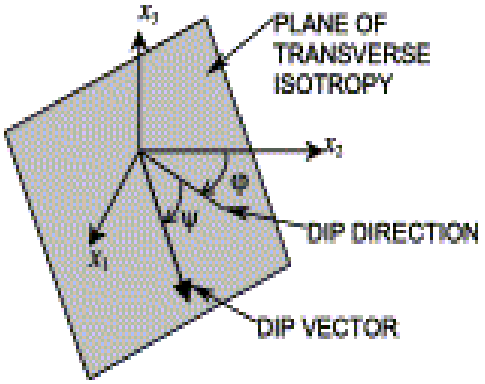

Figure 5. Plane of transverse isotropy with dip direction and dip vector.

There are several types of transverse isotropy. We have transverse isotropy with vertical symmetry axis (VTI), transverse isotropy with a horizontal symmetry axis (HTI) and transverse isotropy with tilted symmetry axis (TTI). The symmetry direction is usually associated with gravity or regional stress. If gravity is the dominant factor, the symmetry direction will be vertical and we get vertical transverse isotropy (VTI). If regional stress is the dominant factor, the symmetry axis can be horizontal, in which we get transverse isotropy with a horizontal symmetry axis (HTI), or the symmetry axis can be tilted with respect to the vertical and horizontal axes, in which case we get tilted transverse isotropy (TTI). The most common physical reason for the HTI symmetry is a system of parallel vertical cracks (fractures), with quasi circular shapes like pennies, embedded in an isotropic matrix (Hudson, 1981; Crampin, 1985; Thomsen, 1988). Basically, modeling and processing of reflection seismic data are more complicated for horizontal transverse isotropy than for vertical transverse isotropy (VTI) media, simply because the azimuthal dependence of moveout velocities and amplitudes in HTI models provides additional information for seismic inversion.

2.4.3. Transverse Isotropy with vertical symmetry axis (VTI)

Most sedimentary rocks can be described by vertical transverse isotropy (VTI) (Thomsen 1986). The simplest physically achievable anisotropic symmetry system is axisymmetric anisotropy, which is generally called Transverse isotropy. Axisymmetry implies that in a given direction, the properties of the medium depend only on the angle between that direction and the symmetry axis. The axis of symmetry is an axis of rotational invariance, about which the formation may be rotated by any angle and still leave the material property the same from what it was before. Figure 6, shows an example of a material with vertical axis of symmetry.

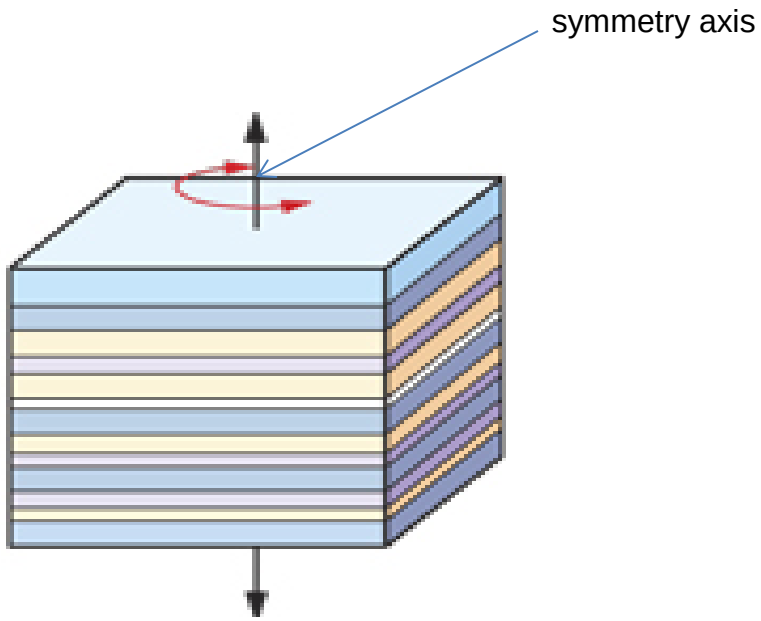

Figure 6. The VTI model has a vertical axis of rotational symmetry and can be caused by small-scale horizontal heterogeneities.

Rock formations with vertical transverse isotropy (VTI) constituent are defined by a stiffness matrix with five independent elements given as;

$$C_{VTI} = \begin{pmatrix} c_{11} & c_{12} & c_{13} & 0 & 0 & 0 \\ c_{12} & c_{11} & c_{13} & 0 & 0 & 0 \\ c_{13} & c_{13} & c_{33} & 0 & 0 & 0 \\ 0 & 0 & 0 & c_{44} & 0 & 0 \\ 0 & 0 & 0 & 0 & c_{44} & 0 \\ 0 & 0 & 0 & 0 & 0 & c_{66} \end{pmatrix}, \quad (6)$$

where $2c_{66} = c_{11} - c_{12}$.

The obtained stiffnesses can be used to re-parameterize into Thomsen notation commonly used in reflection seismology:

$$\varepsilon \equiv \frac{c_{11} - c_{33}}{2c_{33}}, \quad (7)$$

$$\delta \equiv \frac{(c_{13} + c_{44})^2 - (c_{33} - c_{44})^2}{2c_{33}(c_{33} - c_{44})}, \quad (8)$$

$$\gamma \equiv \frac{c_{66} - c_{44}}{2c_{44}}, \quad (9)$$

where Thomsen parameters ($\varepsilon, \delta,$ and γ) are the dimensionless combinations of elastic moduli which characterizes transversely isotropic materials that are encountered in geophysics.

ε is a measure of P- wave anisotropy and the quasi - SV.

δ is responsible for all near vertical P- wave signatures.

γ is required for horizontal shear SH propagation, but has no influence on P- wave propagation.

Also,

$$\varepsilon = \frac{1}{2}\left(\frac{v_{px}^2}{v_{pz}^2} - 1\right), \quad (10)$$

$$\delta = \frac{1}{2}\left(\frac{v_{pn}^2}{v_{pz}^2} - 1\right), \quad (11)$$

$$\gamma = \frac{1}{2}\left(\frac{v_{sx}^2}{v_{sz}^2} - 1\right), \tag{12}$$

where v_{pz}, v_{px} and v_{pn} are vertical, horizontal and normal moveout velocities computed for P – wave, v_{sz} and v_{sx} are vertical and horizontal velocities computed for SH – wave.

2.4.4. Transverse Isotropy with horizontal symmetry axis (HTI)

From Tsvankin (1997), the transversely isotropic model with a horizontal symmetry axis has two mutually orthogonal vertical planes of symmetry. Thus the ''isotropy plane'' (the one normal to the symmetry axis) and the ''symmetry-axis plane'' (the one that contains the symmetry axis).The polarizations of all the three waves in isotropy plane are described by the isotropic equations. Figure 7 shows the horizontal transverse isotropic model with two mutually orthogonal vertical planes of symmetry. The velocities and polarizations in the symmetry-axis plane can be described by analogy with VTI media. The split shear waves in HTI media is denoted as "S^{11}," and "$S^{\perp}$," with the S^{11}-wave polarized in the isotropy plane and the $S^{\perp}$-wave polarization vector being in the plane formed by the symmetry axis and the slowness vector. The superscripts is explained by the fact that in HTI media caused by the parallel vertical cracks, the polarization vector of S^{11} is parallel to the crack planes, while the wave $S^{\perp}$ at vertical incidence is polarized normal to the cracks. In the symmetry axis plane, the S^{11}-wave is polarized in the direction orthogonal to the plane and is called the SH-wave, while $S^{\perp}$ -wave is in-plane motion and is called SV-wave. The mode S^{11} is normally called the "fast" shear wave since at vertical incidence it propagates faster than $S^{\perp}$ (eg., Crampin, 1985).

Figure 7, shows the symmetry plane in HTI media.

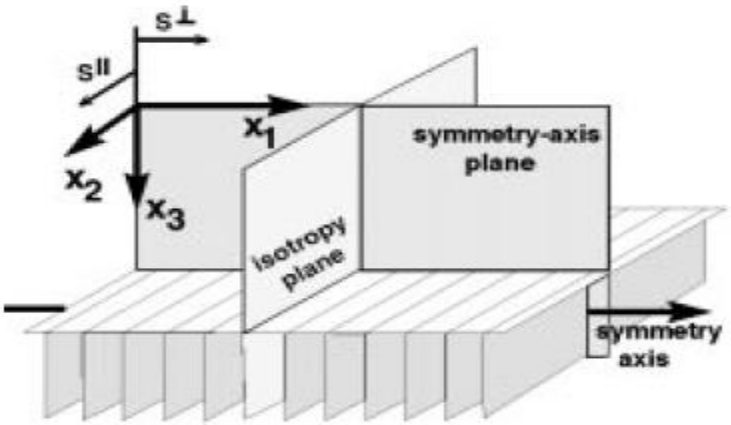

Figure 7. Two vertical symmetry planes in HTI media. In the plane normal to the symmetry axis, velocity is independent of propagation angle. (Tsvankin, 1997)

Figure 8. Photograph of shale showing vertical cracks with horizontal transverse isotropy medium.

Generally, the HTI model is characterized by the stiffness tensor C_{ijkl} that corresponds to the coordinate frame in which x_1 denotes the symmetry axis as shown in fig 7.

Using the Voigt recipe C_{ijkl} can be written as a symmetric 6×6 matrix of the following form:

$$C_{HTI}=\begin{pmatrix} c_{11} & c_{13} & c_{13} & 0 & 0 & 0 \\ c_{13} & c_{33} & (c_{33}-2c_{44}) & 0 & 0 & 0 \\ c_{13} & (c_{33}-2c_{44}) & c_{33} & 0 & 0 & 0 \\ 0 & 0 & 0 & c_{44} & 0 & 0 \\ 0 & 0 & 0 & 0 & c_{55} & 0 \\ 0 & 0 & 0 & 0 & 0 & c_{55} \end{pmatrix}. \tag{13}$$

Alternatively, it is possible to use Thomsen's (1986) parameters defined in a rotated coordinate system with the x_3- axis pointing in the symmetry direction.

2.4.5. Transverse Isotropy with tilted symmetry axis (TTI)

Tilted transverse isotropy is a versatile model of anisotropy, which can be used to obtain formulae describing models with horizontal axes of symmetry. Transverse isotropy with a tilted symmetry axis (TTI media) has been recognized as a common feature of shale formations in overthrust areas. In tilted transverse isotropy media, angles of incidence and reflection are different. When the axis of symmetry and the vertical axis form an angle θ, it is described by the tilted transverse isotropy (TTI) model (Andy Nowacki et al).

A clockwise rotation of the vertical symmetry axis through an angle θ about the y-axis has the orthogonal transformation matrix

$$\begin{pmatrix} \cos\theta & 0 & \sin\theta \\ 0 & 1 & 0 \\ -\sin\theta & 0 & \cos\theta \end{pmatrix}. \tag{14}$$

The corresponding Bond transformation matrix is given by (Auld, 1990; Carcione, 2007),

$$\mathbf{M}=\begin{pmatrix} r_{11}^2 & r_{12}^2 & r_{13}^2 & 2r_{12}r_{13} & 2r_{11}r_{13} & 2r_{11}r_{12} \\ r_{21}^2 & r_{22}^2 & r_{23}^2 & 2r_{22}r_{23} & 2r_{21}r_{23} & 2r_{21}r_{22} \\ r_{31}^2 & r_{32}^2 & r_{33}^2 & 2r_{32}r_{33} & 2r_{31}r_{33} & 2r_{31}r_{32} \\ r_{21}r_{31} & r_{22}r_{32} & r_{23}r_{33} & r_{22}r_{33}+r_{32}r_{23} & r_{23}r_{31}+r_{21}r_{33} & r_{21}r_{32}+r_{31}r_{22} \\ r_{11}r_{31} & r_{12}r_{32} & r_{13}r_{33} & r_{32}r_{13}+r_{12}r_{33} & r_{33}r_{11}+r_{13}r_{31} & r_{31}r_{12}+r_{11}r_{32} \\ r_{11}r_{21} & r_{12}r_{22} & r_{13}r_{33} & r_{12}r_{23}+r_{13}r_{22} & r_{13}r_{21}+r_{23}r_{11} & r_{11}r_{22}+r_{21}r_{12} \end{pmatrix}, \tag{15}$$

where $r_{ij}=\cos(x_i,x'_j)$, $i, j=1, 2, 3$, with x_i and x'_j being the coordinate system before and after rotation, respectively.

Taking into account that

$$\begin{aligned} &r_{11}=r_{33}=\cos\theta \\ &r_{13}=-r_{31}=\sin\theta \\ &r_{22}=1 \\ &r_{12}=r_{21}=r_{23}=r_{32}=0 \end{aligned} \quad , \tag{16}$$

I obtain the Bond matrix that corresponds to the transformation matrix (14),

$$\mathbf{M}=\begin{pmatrix} \cos^2\theta & 0 & \sin^2\theta & 0 & \sin 2\theta & 0 \\ 0 & 1 & 0 & 0 & 0 & 0 \\ \sin^2\theta & 0 & \cos^2\theta & 0 & -\sin 2\theta & 0 \\ 0 & 0 & 0 & \cos\theta & 0 & -\sin\theta \\ -\frac{1}{2}\sin 2\theta & 0 & \frac{1}{2}\sin 2\theta & 0 & \cos 2\theta & 0 \\ 0 & 0 & 0 & \sin\theta & 0 & \cos\theta \end{pmatrix}. \tag{17}$$

Therefore, the stiffness matrix with the rotated symmetry axis is given by

$$\mathbf{C}_{TTI}=\mathbf{M}\mathbf{C}_{VTI}\mathbf{M}^T \ . \tag{18}$$

Substituting matrices (6) and (17) into equation (18) results in the TTI stiffness matrix

$$C_{TTI} = \begin{pmatrix} d_{11} & d_{12} & d_{13} & 0 & d_{15} & 0 \\ d_{12} & d_{22} & d_{23} & 0 & d_{25} & 0 \\ d_{13} & d_{23} & d_{33} & 0 & d_{35} & 0 \\ 0 & 0 & 0 & d_{44} & 0 & d_{46} \\ d_{15} & d_{25} & d_{35} & 0 & d_{55} & 0 \\ 0 & 0 & 0 & d_{46} & 0 & d_{66} \end{pmatrix}. \tag{19}$$

The elements of matrix (19) are

$$\begin{aligned}
d_{11} &= c_{11}\cos^4\theta + 2(c_{13} + 2c_{44})\sin^2\theta\cos^2\theta + c_{33}\sin^4\theta, \\
d_{12} &= c_{12}\cos^2\theta + c_{13}\sin^2\theta, \\
d_{13} &= c_{13}\cos^4\theta + (c_{11} + c_{33} - 4c_{44})\sin^2\theta\cos^2\theta + c_{13}\sin^4\theta, \\
d_{15} &= (-c_{11}\cos^2\theta + c_{33}\sin^2\theta + (c_{13} + 2c_{44})\cos 2\theta)\cos\theta\sin\theta, \\
d_{22} &= c_{11}, \\
d_{23} &= c_{13}\cos^2\theta + c_{12}\sin^2\theta, \\
d_{25} &= -\frac{1}{2}(c_{12} - c_{13})\sin 2\theta, \\
d_{33} &= c_{33}\cos^4\theta + 2(c_{13} + 2c_{44})\sin^2\theta\cos^2\theta + c_{11}\sin^4\theta, \\
d_{35} &= -\frac{1}{4}(c_{11} - c_{33} - (c_{11} + c_{33} - 2c_{13} - 4c_{44})\cos 2\theta)\sin 2\theta, \\
d_{44} &= c_{44}\cos^2\theta + \frac{1}{2}(c_{11} - c_{12})\sin^2\theta, \\
d_{46} &= -\frac{1}{4}(c_{11} - c_{12} - 2c_{44})\sin 2\theta, \\
d_{55} &= c_{44}\cos^2 2\theta + \frac{1}{4}(c_{11} - 2c_{13} + c_{33})\sin^2 2\theta,
\end{aligned} \tag{20}$$

$$d_{66} = \frac{1}{2}(c_{11} - c_{12})\cos^2\theta + c_{44}\sin^2\theta .$$

If $\theta = \pi/2$, the Bond matrix (17) is reduced to

$$\mathbf{M} = \begin{pmatrix} 0 & 0 & 1 & 0 & 0 & 0 \\ 0 & 1 & 0 & 0 & 0 & 0 \\ 1 & 0 & 0 & 0 & 0 & 0 \\ 0 & 0 & 0 & 0 & 0 & -1 \\ 0 & 0 & 0 & 0 & -1 & 0 \\ 0 & 0 & 0 & 1 & 0 & 0 \end{pmatrix}, \tag{21}$$

and the TTI stiffness matrix is transformed into HTI matrix.

For the purpose of the thesis, I considered a TTI medium with tilt in one plane only.

The figure below indicates a TTI model with dip θ and azimuth a.

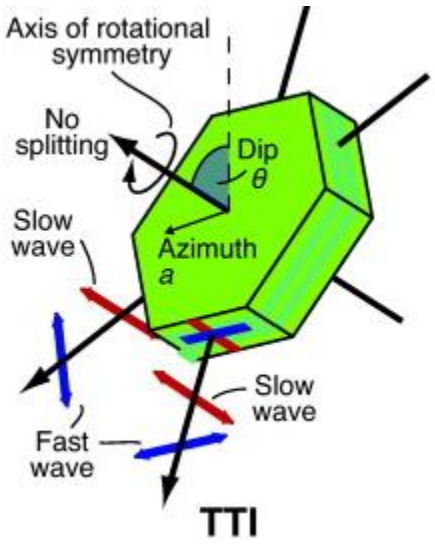

Figure 9. Transverse Isotropy and wave propagation in a medium. The axis is tilted away from the vertical, leading to TTI. The dip θ and azimuth a (the dip direction) of the plane of isotropy define the TTI orientation. (Nowacki et al, 2011)

Figure 10. Photograph of shale outcrop showing a tilted transverse isotropy medium.

2.5. Effective medium

The subject of effective media theories for fractured reservoirs is important in exploration seismology, since it may reveal information about permeability anisotropy and therefore about the preferred direction of the fluid flow (Grechka and Kachanov, 2006a, b). The complexity of the reservoir structure (layering and fracture orientations) requires the use of tangible rheologies, so the fracture trend is to pass from simple symmetries, such as transverse isotropy, to lower anisotropic symmetries (eg., orthorhombic and monoclinic) (Tsvankin et al., 2010). If we consider a layered medium composed of layers of arbitrary anisotropy in welded contact (Figure 11), here we assume thin layers and stationarity. The $x_3 - axis$ is perpendicular to the layering. Each constituent has, relative to the total thickness of all the constituents, a cumulative thickness $t_i, i = 1,...,n$ (with $t_1 + ... + t_n = 1$), a density ρ_i, and an elastic modulus tensor whose elements C_{pqrsi} relative to stress σ_{pqi} to strain ε_{rsi} according to the generalized Hooke's law, $\sigma_{pqi} = C_{pqrsi}\varepsilon_{rsi}$. In a notation form where $C_{pqrsi} = C_{jki}$ according to the

convention $11 \to 1,\quad 22 \to 2,\quad 33 \to 3,\quad 23 \to 4,\quad 31 \to 5$ and $12 \to 6$ the convention on strains that $[\varepsilon_1, \varepsilon_2, \varepsilon_3, \varepsilon_4, \varepsilon_5, \varepsilon_6] \equiv [\varepsilon_{11}, \varepsilon_{22}, \varepsilon_{33}, \varepsilon_{23}, \varepsilon_{31}, \varepsilon_{12}]$, the stress – strain relation in a layer of the i^{th} constituent can be written

$$\sigma_{ji} = \sum_{k=1}^{6} C_{jki} \varepsilon_{ki}, \quad j = 1, \cdots, 6. \tag{22}$$

The elastic moduli for the long-wavelength equivalent anisotropic medium can be expressed in terms of thickness weighted averages of functions of the moduli of the constituents.

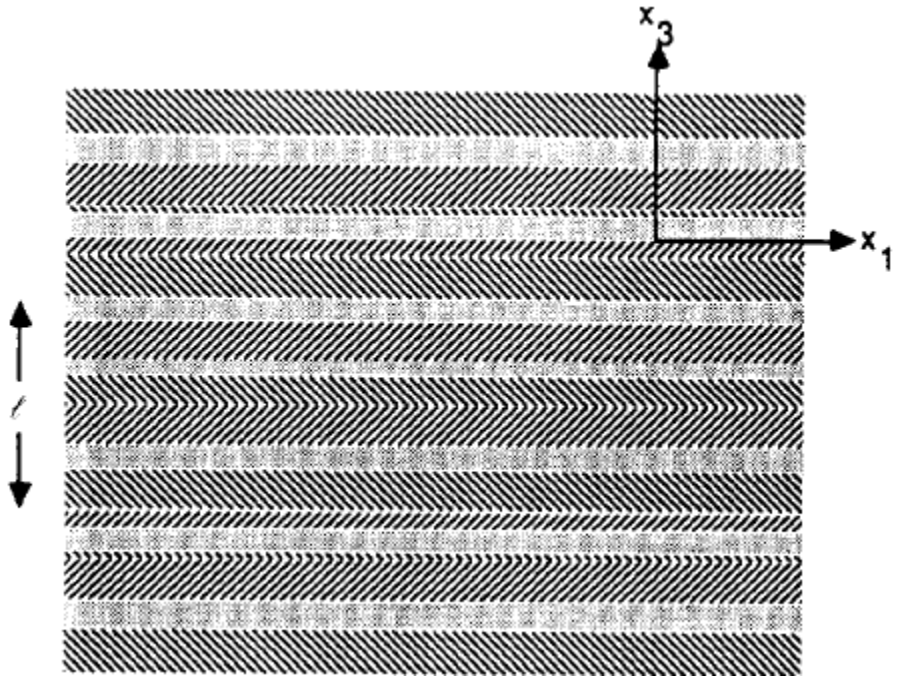

Figure 11. A stack of layers consisting of three constituents. Each constituent may be anisotropic. In any interval of thickness l or larger, where l is much smaller than a wavelength, the percentage of each constituent is assumed to be stationary with respect to the vertical coordinate x_3.

On the other hand, Backus (1962) averaging is also based on the effective medium theory, i.e. the effective elastic modulus represents an equivalent homogeneous medium which have the same elastic properties. The elastic properties of the effective medium depend on the degree of the vertical heterogeneity (Berryman et al 1999) and

the length of averaging (Sams and Williamson 1994, Liner and Fei 2006). The length of the averaging should be long enough so that properties of the medium are nearly independent for the vertical direction after smoothing.

2.6. Backus Averaging

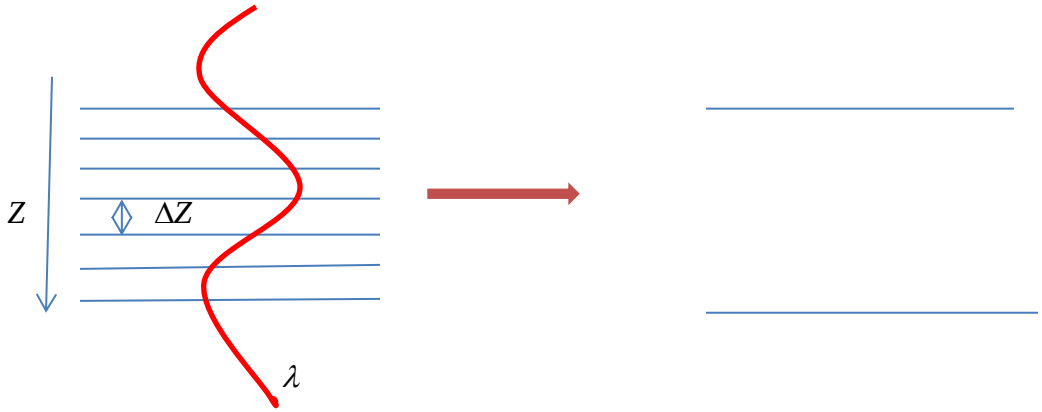

Figure.12(a). A horizontally layered inhomogeneous medium.

12 (b). A homogeneous medium.

Backus averaging implies a harmonic mean of elastic moduli of well logs in a desired depth thickness.

Backus (1962) presented an equivalent medium theory, thus a heterogeneous medium can be replaced by a homogeneous one which will predict the wave propagation in the actual medium. From figure 12(a), the horizontally layered medium is upscaled from inhomogeneous to a homogeneous one, figure 12 (b). That is when $\lambda >> \Delta Z$. Where λ is the wavelength and ΔZ is the layer thickness.

The geological model above consists of a layered equally spaced vertical transverse isotropy medium with **N** layers. The Backus (1962) averaging gives the effective system matrix $\tilde{\mathbf{M}}$ given by a simple arithmetic averaging of all system matrices $\mathbf{M}_j$ from the

stack of **N** layers. The Backus averaging method (Backus 1962) considers the thickness (ΔZ) of the stack of layers to be smaller than the source wavelength.

Backus, used a simple arithmetic averaging

$$\tilde{\mathbf{M}} = \langle \mathbf{M} \rangle = \frac{1}{N} \sum_{j=1}^{N} \mathbf{M}_j \,, \tag{23}$$

to compute the effective medium. The standard Thomsen (1986) notations are used to compute the elements of matrices $\mathbf{M}_j$. The notations are;

$$\begin{aligned}
c_{33j} &= \rho_j v_{pj}^2 \,, \\
c_{44j} &= \rho_j v_{sj}^2 \,, \\
c_{11j} &= c_{33j}(1+2\varepsilon_j)\,, \\
c_{13j} &= \sqrt{(c_{33j}-c_{44j})\left(c_{33j}(1+2\delta_j)-c_{44j}\right)} - c_{44j} \,, \\
c_{66j} &= c_{44j}(1+2\gamma_j).
\end{aligned} \tag{24}$$

where c_{11j}, c_{13j}, c_{33j}, c_{44j} and c_{66j} are the elements of the stiffness matrix. The effective VTI medium properties are computed from the elements of matrix, $\tilde{\mathbf{M}}$. For a given formation, the arithmetic averaging operators are;

$$\begin{aligned}
\tilde{c}_{11} &= \left\langle c_{11} - \frac{c_{13}^{\,2}}{c_{33}} \right\rangle + \left\langle \frac{c_{13}}{c_{33}} \right\rangle^2 \left\langle c_{33}^{\,-1} \right\rangle^{-1}, \\
\tilde{c}_{13} &= \left\langle \frac{c_{13}}{c_{33}} \right\rangle \left\langle c_{33}^{\,-1} \right\rangle^{-1}, \\
\tilde{c}_{33} &= \left\langle c_{33}^{\,-1} \right\rangle^{-1}, \\
\tilde{c}_{44} &= \left\langle c_{44}^{\,-1} \right\rangle^{-1}, \\
\tilde{c}_{66} &= \langle c_{66} \rangle, \\
\tilde{\rho} &= \langle \rho \rangle
\end{aligned} \tag{25}$$

For practical purposes, Liner and Fei (2006) recommend the length of averaging to be less than or equal to one-third of the minimum dominant wavelength.

Moreover, according to Mavko et al (1998) individual layer thickness must be at least ten times smaller than the source wavelength. Periodicity of layers is not required and individual layers can be either isotropic or anisotropic. The Backus averaging equations were developed for layered models with isotropic and VTI layer constituents only. Backus (1962) developed relatively straightforward expressions for the five elastic constants ($c_{11}, c_{13}, c_{33}, c_{44}, c_{66}$) of the effective TI medium from volume averages of the elastic properties of the individual layers.

2.7. Shoenberg – Muir Theory

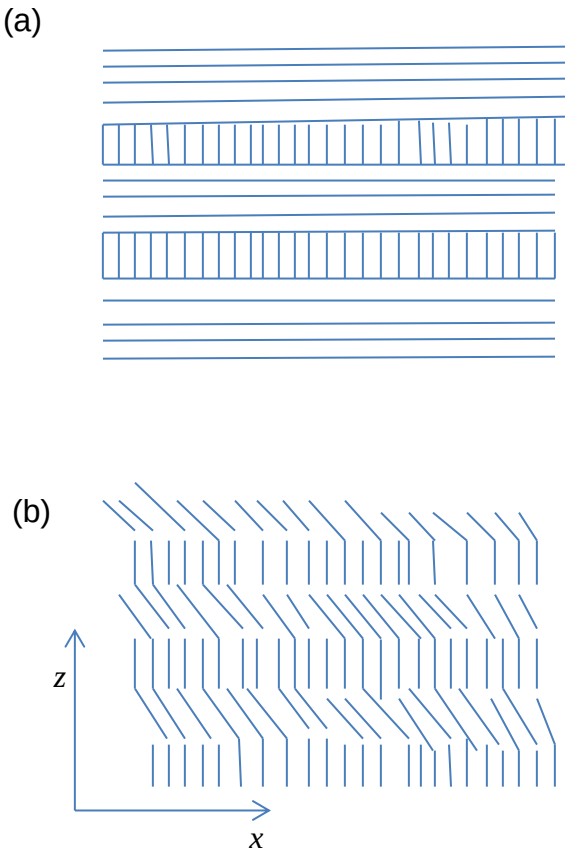

Figure 13. Stack of thin (compared to the wavelength) strata composed of HTI and VTI layers (a) and 45TI and VTI layers (b). the percentage of each constituent is assumed to be stationary with respect to the vertical coordinate.

The Schoenberg – Muir (1989) theory states that an equivalent, homogeneous and anisotropic medium can be constructed from a layered medium composed of several thin layers, each anisotropic under the assumption of stationarity. To test the theory, we consider single transversely isotropic layers with different orientations of the symmetry axis and perform numerical simulations. Let us consider a finely layered medium composed of **N** arbitrarily anisotropic layers (Figure 13), with the z-axis perpendicular to the layering plane. Each layer is defined by density ρ, volume fraction α and elastic constants, c_{ij}. The stiffness matrix for arbitrary anisotropy is written as;

$$\mathbf{C} = \begin{pmatrix} c_{11} & c_{12} & c_{13} & c_{14} & c_{15} & c_{16} \\ c_{21} & c_{22} & c_{23} & c_{24} & c_{25} & c_{26} \\ c_{31} & c_{32} & c_{33} & c_{34} & c_{35} & c_{36} \\ c_{41} & c_{42} & c_{43} & c_{44} & c_{45} & c_{46} \\ c_{51} & c_{52} & c_{53} & c_{54} & c_{55} & c_{56} \\ c_{61} & c_{62} & c_{63} & c_{64} & c_{65} & c_{66} \end{pmatrix}, \tag{26}$$

with only 21 independent elements. The stiffness matrix (26) can be written in terms of four submatrices as

$$\mathbf{C} = \begin{pmatrix} \mathbf{C}_{TT} & \mathbf{C}_{TN} \\ \mathbf{C}_{TN}^{T} & \mathbf{C}_{NN} \end{pmatrix}, \tag{27}$$

where

$$\mathbf{C}_{NN} = \begin{pmatrix} c_{33} & c_{34} & c_{35} \\ c_{34} & c_{44} & c_{45} \\ c_{35} & c_{45} & c_{55} \end{pmatrix}, \tag{28}$$

$$\mathbf{C}_{TN} = \begin{pmatrix} c_{13} & c_{14} & c_{15} \\ c_{23} & c_{24} & c_{25} \\ c_{36} & c_{46} & c_{56} \end{pmatrix}, \tag{29}$$

$$\mathbf{C}_{TT} = \begin{pmatrix} c_{11} & c_{12} & c_{16} \\ c_{12} & c_{22} & c_{26} \\ c_{16} & c_{26} & c_{66} \end{pmatrix}, \tag{30}$$

and $\mathbf{C}_{TN}^{T}$ is transpose of matrix $\mathbf{C}_{TN}$.

According to Schoenberg and Muir (1989), the equivalent homogeneous medium is defined by the following matrix

$$\tilde{C} = \begin{pmatrix} \tilde{C}_{TT} & \tilde{C}_{TN} \\ \tilde{C}_{TN}^{T} & \tilde{C}_{NN} \end{pmatrix}, \tag{31}$$

where

$$\tilde{C}_{NN} = \left\langle C_{NN}^{-1} \right\rangle^{-1}, \tag{32}$$

$$\tilde{C}_{TN} = \left\langle C_{TN} C_{NN}^{-1} \right\rangle \left\langle C_{NN}^{-1} \right\rangle^{-1}, \tag{33}$$

$$\tilde{C}_{TT} = \left\langle C_{TT} \right\rangle - \left\langle C_{TN} C_{NN}^{-1} C_{TN}^{T} \right\rangle + \left\langle C_{TN} C_{NN}^{-1} \right\rangle \left\langle C_{NN}^{-1} \right\rangle^{-1} \left\langle C_{NN}^{-1} C_{TN}^{T} \right\rangle, \tag{34}$$

and the thickness (volume fraction) weighted matrix average is defined as

$$\langle \mathbf{C} \rangle = \sum_{j=1}^{N} \alpha_j \mathbf{C}_j \tag{35}$$

with $\sum_{j=1}^{N} \alpha_j = 1$.

CHAPTER THREE

3.0 Upscaling in seismics

Well- log data need upscaling to seismic frequency and the upscaling is normally than with Backus averaging (Backus 1962). Shale plays an important role in fluid flow and seismic wave propagation because of its low permeability and anisotropic microstructure (Sayers 2005). Shale is composed of clay minerals and these are intrinsically vertical transverse isotropy (VTI) anisotropic (Banik 1984). For the purpose of the thesis, I used a generalized analytical expression of Backus (1962) averaging for a stack of anisotropic thin layers by Schoenberg and Muir (1989), to derive explicit analytical formulae for common layer models with layer constituents that are; vertical transverse isotropy (VTI), horizontal transverse isotropy (HTI) and tilted transverse isotropy (TTI). The Intrabasalt 2 formation selected for the upscaling were modeled into different forms and analyzed subsequently.

3.1 Methodology

Basically, two methods were used for the upscaling. I used Backus averaging method (Backus 1962) and Schoenberg-Muir (1989) method. Backus averaging method (Backus 1962) considers the thickness (N) of stack of layers to be smaller than the source wavelength. The formation selected for the upscaling is Intrabasalt 2 formation and contains parameters such as v_{po}, v_{so} , density, and anisotropy parameters epsilon (ε), delta (δ) and gamma (γ). The Backus averaging was used to;

(1) Calculate the stiffnesses c_{11}, c_{12} , c_{13} , c_{33} , c_{44} and c_{66}.
(2) Analyse the VTI-VTI test.
(3) Determine the effective properties versus net to gross.

On the other hand, the Schoenberg –Muir (1989) method also considers periodic systems of equal composition whose single layers have transversely isotropic symmetry (VTI) with different orientations of the symmetry axis. The parameters used for the

Schoenberg-Muir theory were v_{po}, v_{so}, density, and anisotropy parameters epsilon (ε), delta (δ), gamma (γ) and tilt.

The Schoenberg –Muir (1989) theory was used to;

(1) Determine the effective properties versus tilt in sand using the whole Intrabasalt 2 formation.

(2) Analyse the VTI-HTI test.

(3) Analyse the VTI-TTI 45° test.

3.1.1. Backus averaging method

I used well log data from the North Sea for the write up. The data contains eight feasible formations, thus Flett, Basalt 1, Intrabasalt 1, Intrabasalt 2, Intrabasalt, Hyaloclastic, Basalt and Lamba. The formations can be seen in figure 14. The formation selected for the Backus averaging and upscaling is intrabasalt 2 formation. It consists of 1063 layers and the total depth of the formation is 161.849 m.

The formation starts at the depth of 1760.481 m and ends at 1922.33 m. The medium consists of thin isotropic layers with P- and S- wave velocity, density and the anisotropy parameters epsilon (ε), delta (δ) and gamma (γ). The stiffnesses, c_{11}, c_{12}, c_{13}, c_{33}, c_{44} and c_{66} were computed for the individual layers using equations (20) and (21).

The stiffnesses were cross plotted against the depth and the models obtained were analyzed to find places of high stiffnesses and low stiffnesses. Figure 18 depicts the models obtained. The figures and their interpretation can be seen in chapter four.

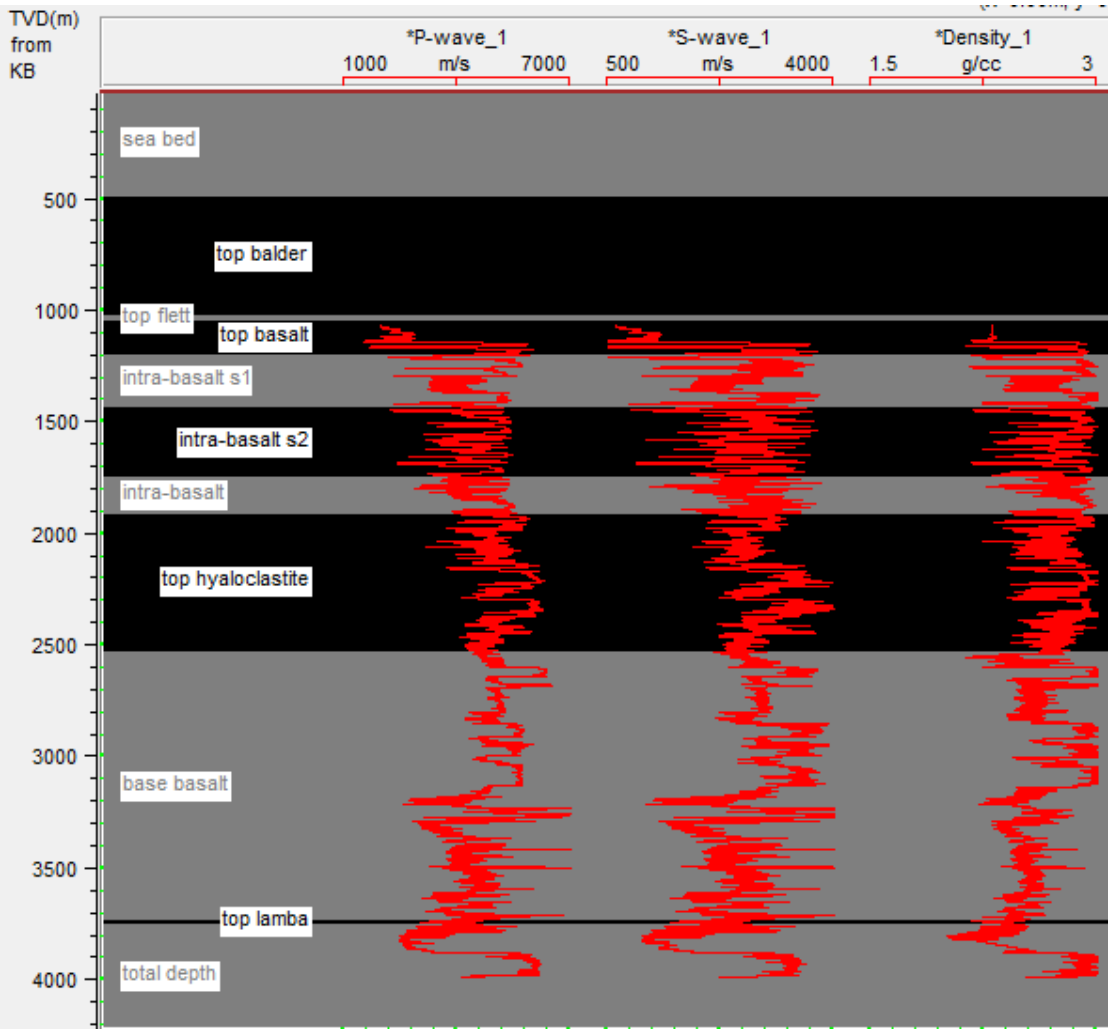

Figure 14. Sonic v_p, v_s and density logs of the eight formations.

3.1.2 Shoenberg-Muir method

For the purpose of the thesis, I assume the Intrabasalt 2 formation is a stack of N thin arbitrarily anisotropic layers with z-axis perpendicular to the layering plane. The Intrabasalt 2 data was modeled using matlab algorithm. The effective properties versus tilt in sand were determined. In addition, the VTI - HTI and VTI – TTI 45° against net to gross were also determined using values from table 1.

3.2 Discrimination between sand and shale

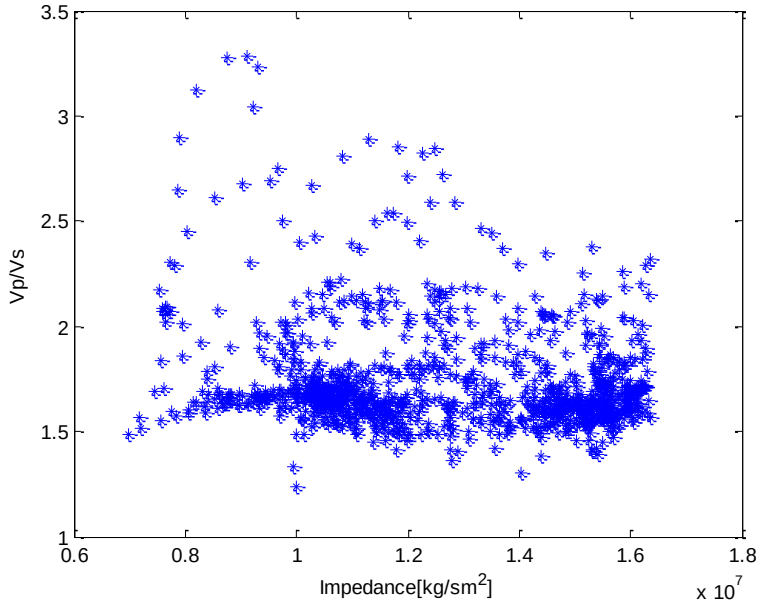

15)

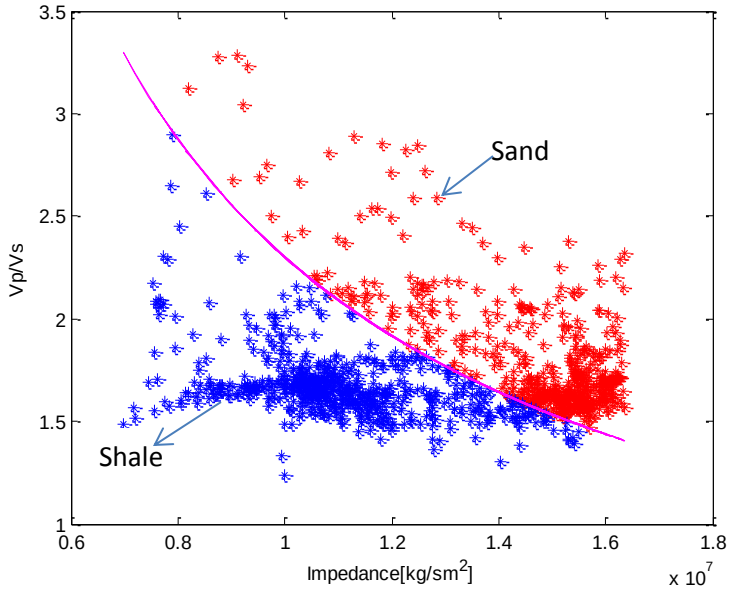

16)

Figures 15 and 16. Cross plot of V_p/V_s-ratio and acoustic impedance. (15) Cross plot of V_p/V_s against acoustic impedance of Intrabasalt 2 formation. (16) Cross plot of V_p/V_s against acoustic impedance showing that different lithologies have different V_p/V_s ratios.

The most paramount difficulty in geological modeling is to take proper account of the various large to small-scale heterogeneities. We have large scale faults, micro cracks, cracks, fractures etc. Each type of heterogeneity influences fluid flow and for that matter there is the need for upscaling (Webber et al., 1990). The major tasks in seismic exploration are to obtain high quality images of the subsurface structures and to discriminate between different lithologies (Landrø, 2012). Our main target is to discriminate between sand and shale, simply because sand and shale might have the same acoustic impedance, therefore if we are not able to discriminate between the two lithologies, there is the probability of missing our target zone. Practical investigations show that shale has higher V_p/V_s ratios than sands. In order to discriminate between sand and shale, acoustic impedance and the ratio of V_p/V_s should be known. The product of seismic velocities and the mass density is called impedances. The P-wave acoustic impedance is the product of P-wave velocity and density and the S-wave acoustic impedance is the product of S-wave velocity and density. Fig 15 shows a crossplot of V_p/V_s ratio against acoustic impedance. The Intrabasalt 2 data was used for the modeling. The data was loaded into matlab and computations were carried out. In order to discriminate between the two lithologies, an optimum constant of 2.3×10^7 was selected and the acoustic impedances of the individual layers were plotted against the optimum constant divided by the individual impedances. The pink line above was obtained as a result of the computation (fig. 16). Also, every point above the pink line was assigned flag one, which represents sand and every point below the pink line was assigned flag zero which represents shale. The source code can be found in appendix. As can be seen from Fig 16, the red part represent sand and the blue part represent shale. I am using sand and shale, simply because research has shown that shale is intrinsically isotropic (VTI) while sandstone is intrinsically anisotropic (HTI). Also porosity and permeability are petrophysical parameters needed to quantify the mass and recoverability of oil and gas in reservoirs. Therefore there is the need for us to estimate the voids, cracks, fractures etc in the reservoirs. For instance, the size of voids in shale rock can vary by a few orders of magnitude from a few millimeters to a few nanometers. In the same way, the heterogeneity of gas shale comes not only from large scale

variation of pores and cracks during rock formation or compaction, but also from porous kerogen material in various stages of maturity. These heterogeneities cause nonuniformity and anisotropy of transport and mechanical properties such as porosity, permeability, wettability and absorption (Zhang et al, 2012). Due to that we have to integrate the information such as porosity and permeability extracted from the data at very small scale with the larger scale, ie, upscaling.

3.3 Sand –Shale Intercalation

Every flag has its depth, v_p, v_s, density, anisotropic parameters , $\varepsilon, \delta,$ and γ, stiffnesses $c_{11}, c_{12}, c_{13}, c_{33}, c_{44}$ and c_{66}. The data was modeled again into sand–shale intercalation using matlab algorithm. The density and the stifffnesses were plotted against the depth. Figure 19, represents the models. Each model was analyzed and upscaled to find places of larger sands, high stiffnesses, low shale and vice versa.

3.4. Selection of sand –shale representatives and their analysis

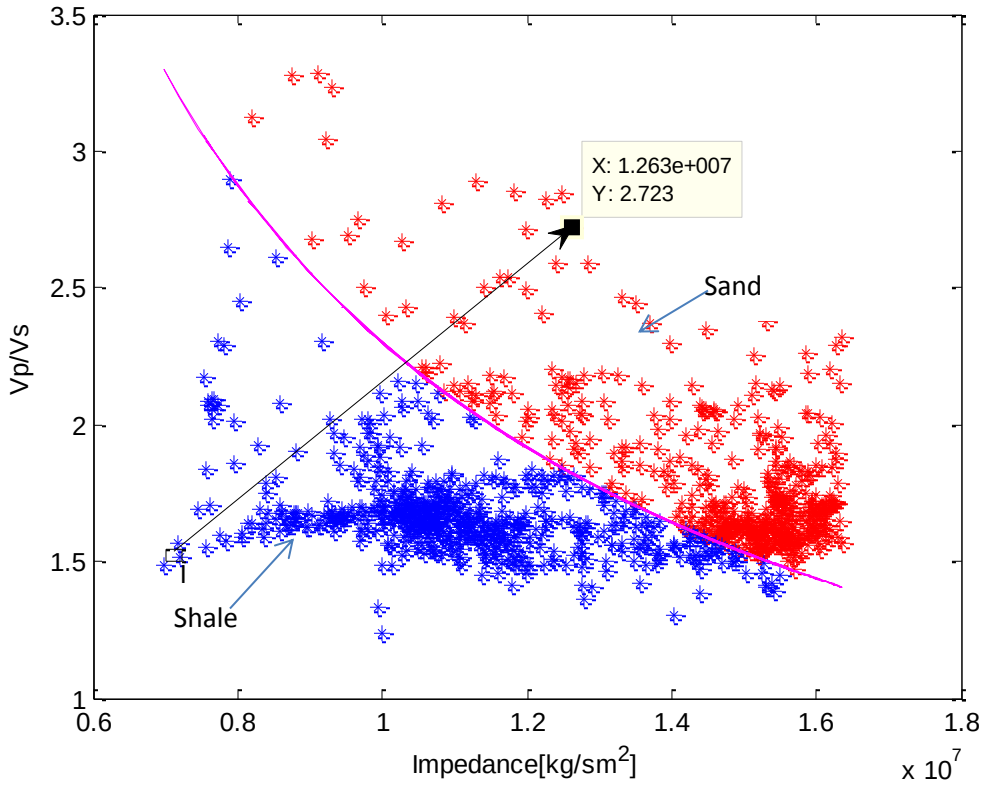

Figure 17. Model showing selection of sand-shale representation.

Two points were selected from the model. One from each lithology. The points selected are indicated by the black arrows. Their stiffnesses and density were located from the model parameters and tabulated. The table below shows the lithology, stiffnesses and density of the selected points.

Lithology	c_{11}(GPa)	c_{12}(GPa)	c_{13}(GPa)	c_{33}(GPa)	c_{44}(GPa)	c_{66}(GPa)	Density (g/cc)
Sand	62.10	45.20	44.70	60.80	8.19	8.44	2.62
Shale	24.50	2.14	3.45	20.90	9.11	11.10	2.47

Table 1. Rock properties of lithology used to compute Backus averaging and Schoenberg –Muir averaging.

3.4.1 VTI – VTI and Net to Gross (N/G) test

Table 1 was used to perform the VTI –VTI test. Net to gross (N/G) is the ratio of porous and permeable rocks to non-porous and non-permeable rocks in the reservoir. Thus the (N/G) indicates the amount of sand that can pay or the amount of sand that is sensitive to fluids. I used the Backus (1962) average effective medium theory to estimate the effective, upscaled anisotropic properties of the interbedded sand-shale sequences. I did it for different net to gross (N/G) values, ranging from 0 to 1. The first part of the averaging formulae represents sand while the second part represents shale. The first part of the averaging is a product of (N/G) and the averaging formulae while the second part is a product of (1- N/G) and the averaging formulae. Finally, the effective properties were computed and cross-plotted against net to gross (N/G). Matlab algorithm was used to compute the data numerically. The source code can be found in appendix. Figure 20, shows the models obtained.

3.4.2. VTI - HTI and Net to Gross (N/G) test

The Shoenberg - Muir formulae was used for the VTI - HTI test to estimate the effective, upscaled anisotropic properties of the interbedded sand-shale sequence. The effective properties were computed and cross-plotted against net to gross (N/G). Figure 21, depicts the models. The source code can be found in appendix.

3.4.3. VTI - TTI 45° and Net to Gross (N/G) test

The Schoenberg – Muir formulae was used for the VTI - TTI 45° test. This is a special case when we considered the tilt angle of the symmetry axis,

$$\theta = \frac{\pi}{4} \text{ .} \tag{36}$$

After the computation, the effective properties were cross-plotted against net to gross (N/G). Figure 22, demonstrates the models.

3.4.4. Effective properties versus tilt in sand

This is a special case when the whole intrabasalt 2 formation was considered as sand, which is a bit different from the previous ones. After the computation, the effective properties were cross-plotted against the tilt angles. Figure 23 shows the models.

CHAPTER FOUR

4.0 Results and Discussion

Effective properties and stiffnesses with depth

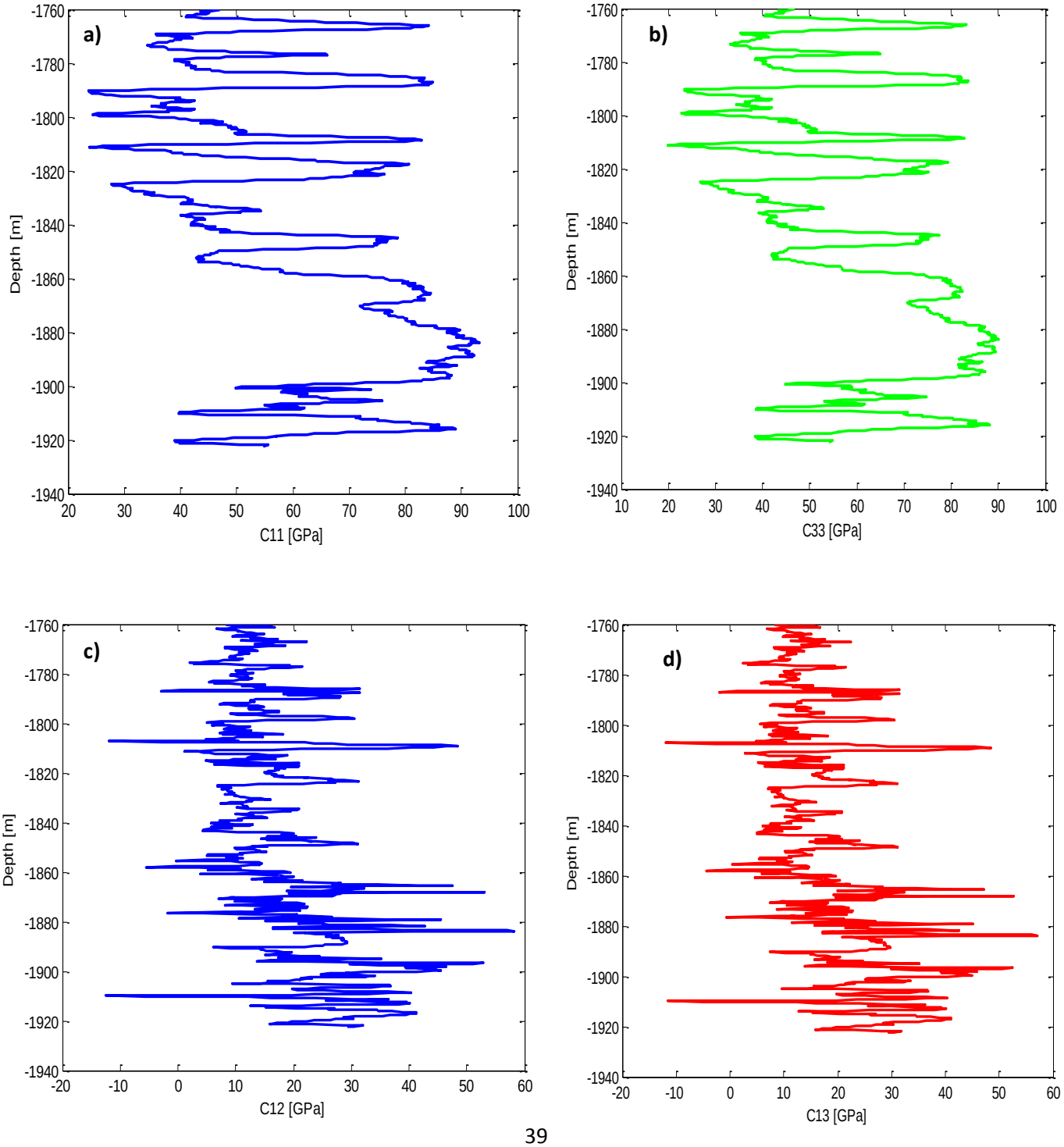

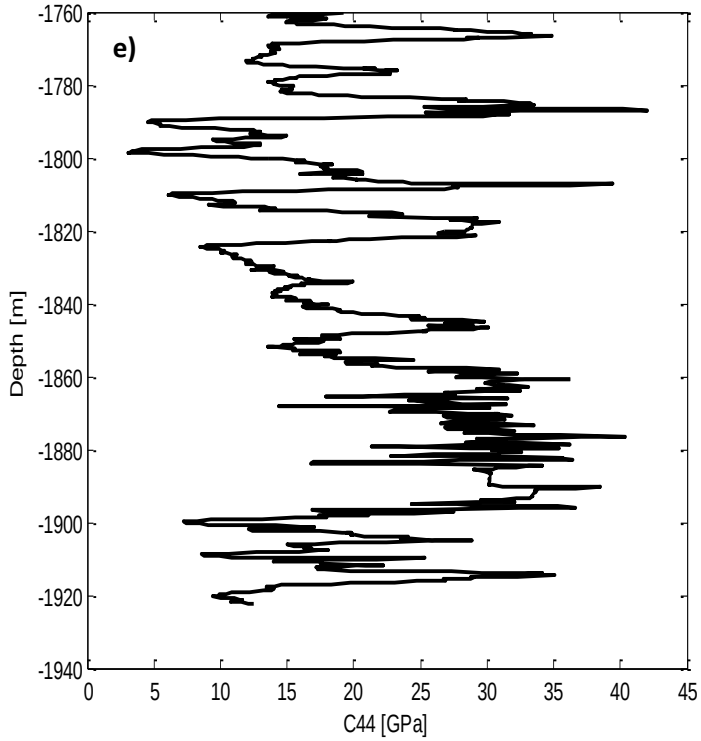
e)
Depth [m]
C44 [GPa]

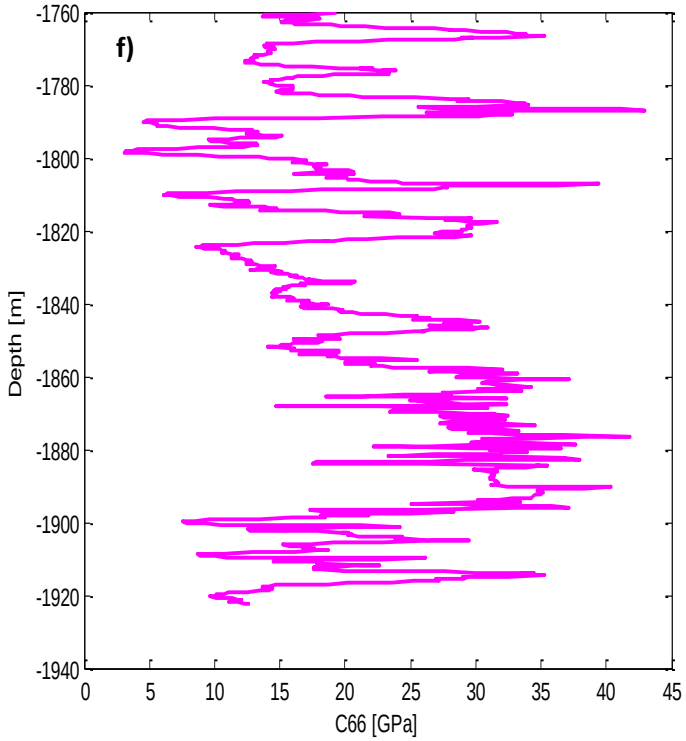
f)
Depth [m]
C66 [GPa]

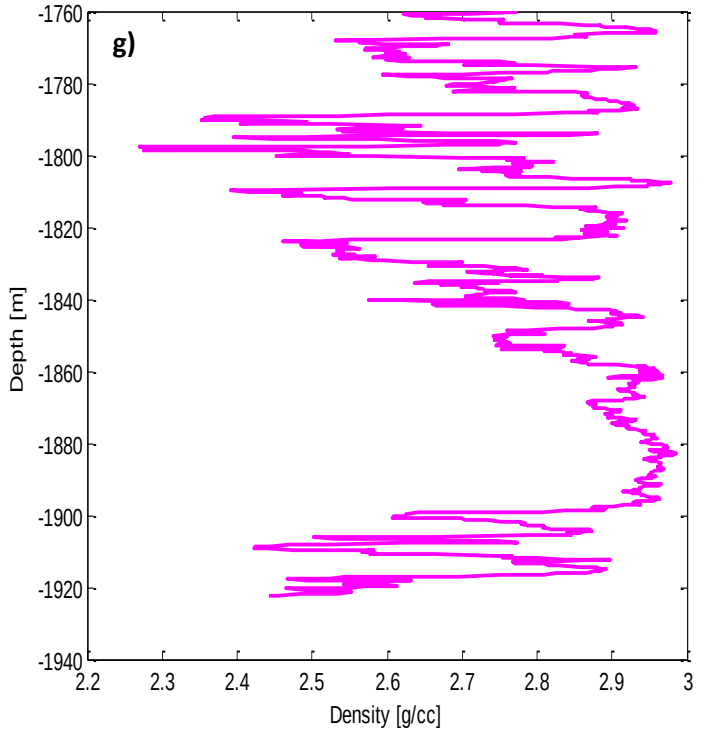
g)
Depth [m]
Density [g/cc]

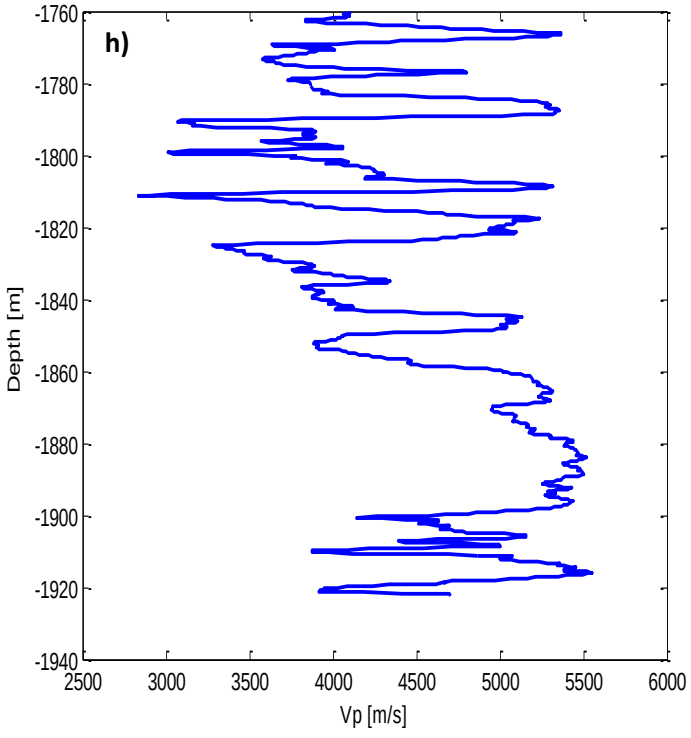
h)
Depth [m]
Vp [m/s]

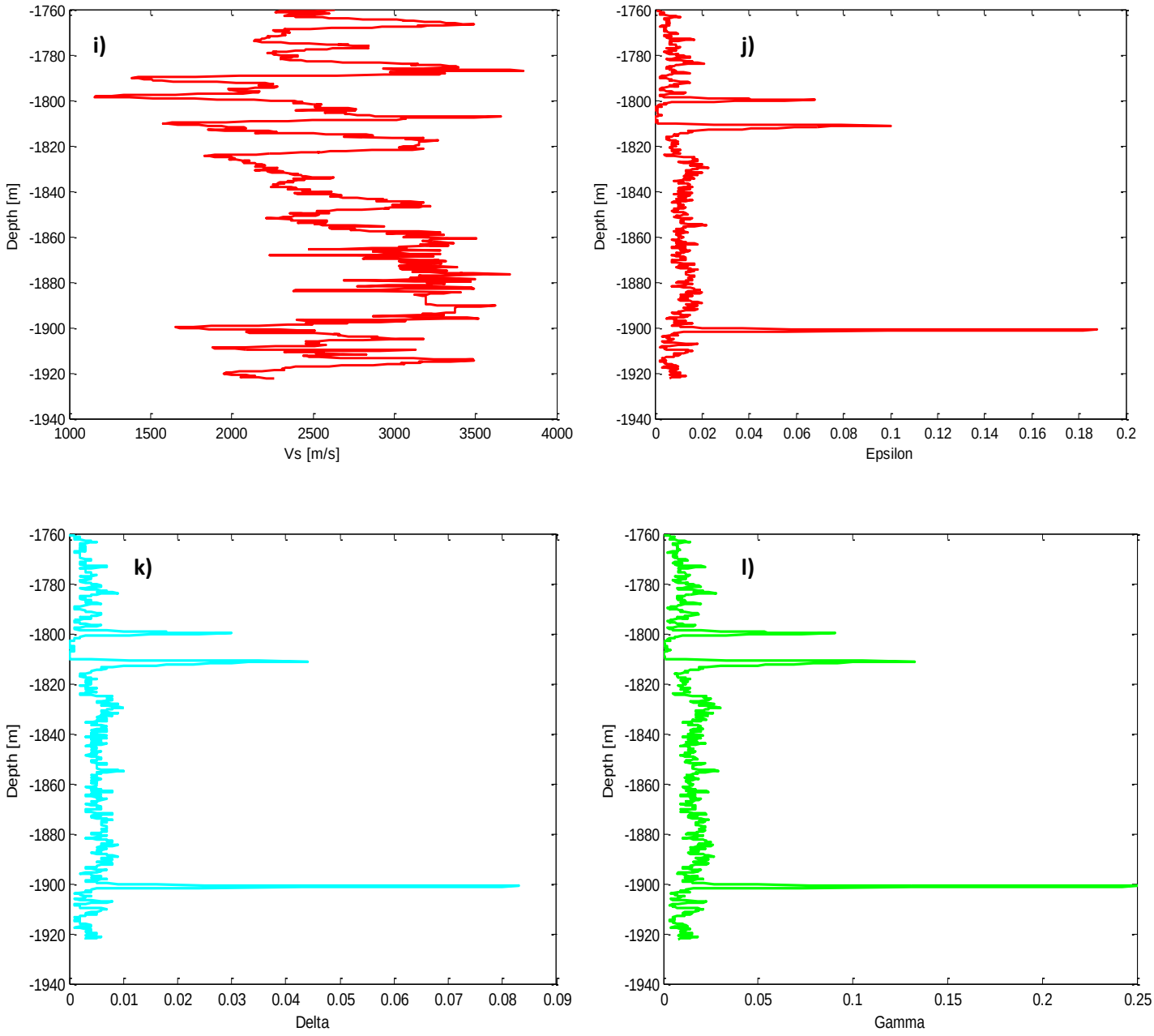

Figure 18. Models of effective properties and stiffnesses with depth of formation. (a) stiffness c_{11} versus depth of formation. (b) stiffness, c_{33} versus depth of formation. (c) stiffness, c_{12} versus depth of formation. (d) stiffness, c_{13} versus depth of formation. (e) stiffness, c_{44} versus depth of formation. (f) stiffness, c_{66} versus depth of formation. (g) effective property, density versus depth of formation. (h) effective property, v_p versus depth of formation. (i) effective property, v_s versus depth of formation. (j) anisotropic parameter, epsilon versus depth of formation. (k) anisotropic parameter, delta versus depth of formation. (l) anisotropic parameter, gamma versus depth of formation.

From fig. 18 a, the stiffness tensor c_{11} is very high at a depth range of 1765 m –1770 m, 1780 m – 1790 m and most pronounced at 1880 m – 1990 m. The highest stiffness range between [80 – 90] GPa. The stiffness tensor c_{33} is also very high at depth range of 1765 m – 1770 m, 1780 m – 1790 m and pronounced at 1880 m – 1990 m. Comparing the two figures, thus fig. 18 a and 18 b, I can infer that they have the same behavior and the same properties with depth of formation. Looking at fig. 18 c, the stiffness tensor c_{12} started increasing with depth up to 1770 m and decreases gradually to 1780 m. It continues increasing and decreasing throughout the formation. The highest stiffness occurs at the depth 1880 m – 1882 m, with stiffness of [15 – 58] GPa. The behavior of c_{12} is virtually the same as c_{13}. On the other hand, c_{44} and c_{66} show almost the same behavior with the highest stiffness ranging between [40-44] GPa. The stiffness started increasing and decreasing up to a depth of 1868 m. It then remained constant at the depth 1870 m – 1876 m. This can be as a result of the sediments being homogeneous within the depth. Fig. 18 g, also indicates the density profile, with the highest density falling within the depth range of 1880 m – 1900 m. The density profile started increasing from the surface of the formation up to 1770 m and decreases gradually to 1775 m. It continued increasing and decreasing with depth , with the highest density occurring at the depth of 1880 m – 1900 m and the lowest at the depth of 1795 m – 1800 m. The density might be higher as a result of the formation being more compact, less porous, and without voids and cracks etc. The effective property v_p also exhibited the same behavior. From the model, v_p is highest at the depth of 1880 m – 1900 m which might be due to the increase in fluid saturation. Therefore, I can conclude that the higher the density, the higher the v_p. Comparing the stiffnesses with the density, I can infer that the higher the density, the higher the stiffness within the formation. Area of high v_p is also an indication of low stiffness. From (i), I could see that the v_s is very low at a depth of 1788 m – 1800 m, which might be decreasing fluid saturation.

The anisotropic parameters also give an indication of high and low stiffnesses. The values of the parameter delta (δ) estimated from the well lies within the range

$0 \le \delta \le 0.09$. The values of the parameter epsilon (ε) and gamma (γ) also lie within the ranges of $0 \le \varepsilon \le 0.2$, $0 \le \gamma \le 0.25$ respectively. At a depth of 1895 m - 1905 m, all the anisotropic parameters were very high, and then decreases abruptly within a depth range of 1815 m - 1890 m. Comparing with the stiffnesses, I could see a pattern which they all follow. Thus, when the anisotropic value is very high, there is the likelihood of the stiffness also being very high within the medium.

Intercalation of Sand-Shale with Depth

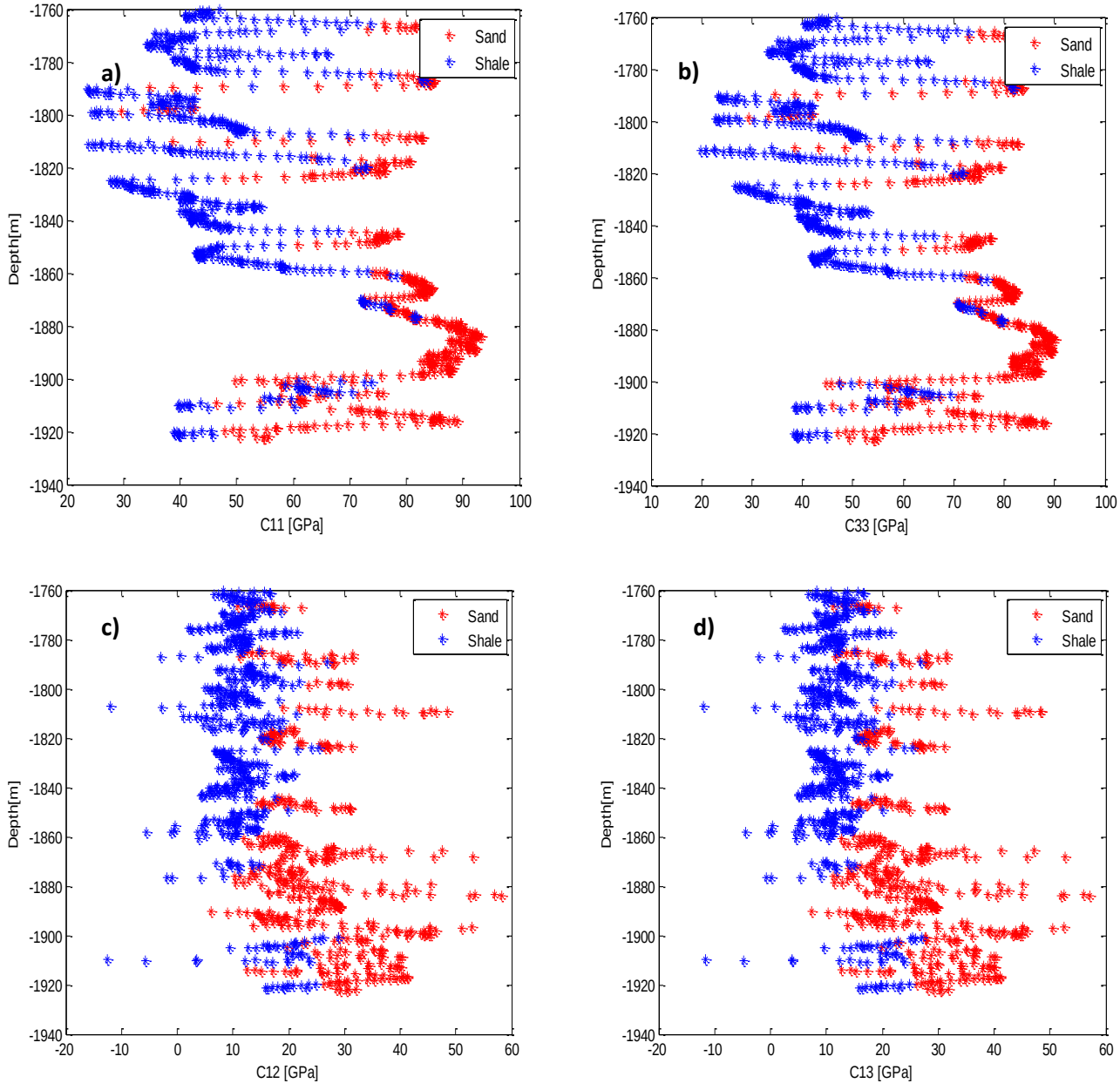

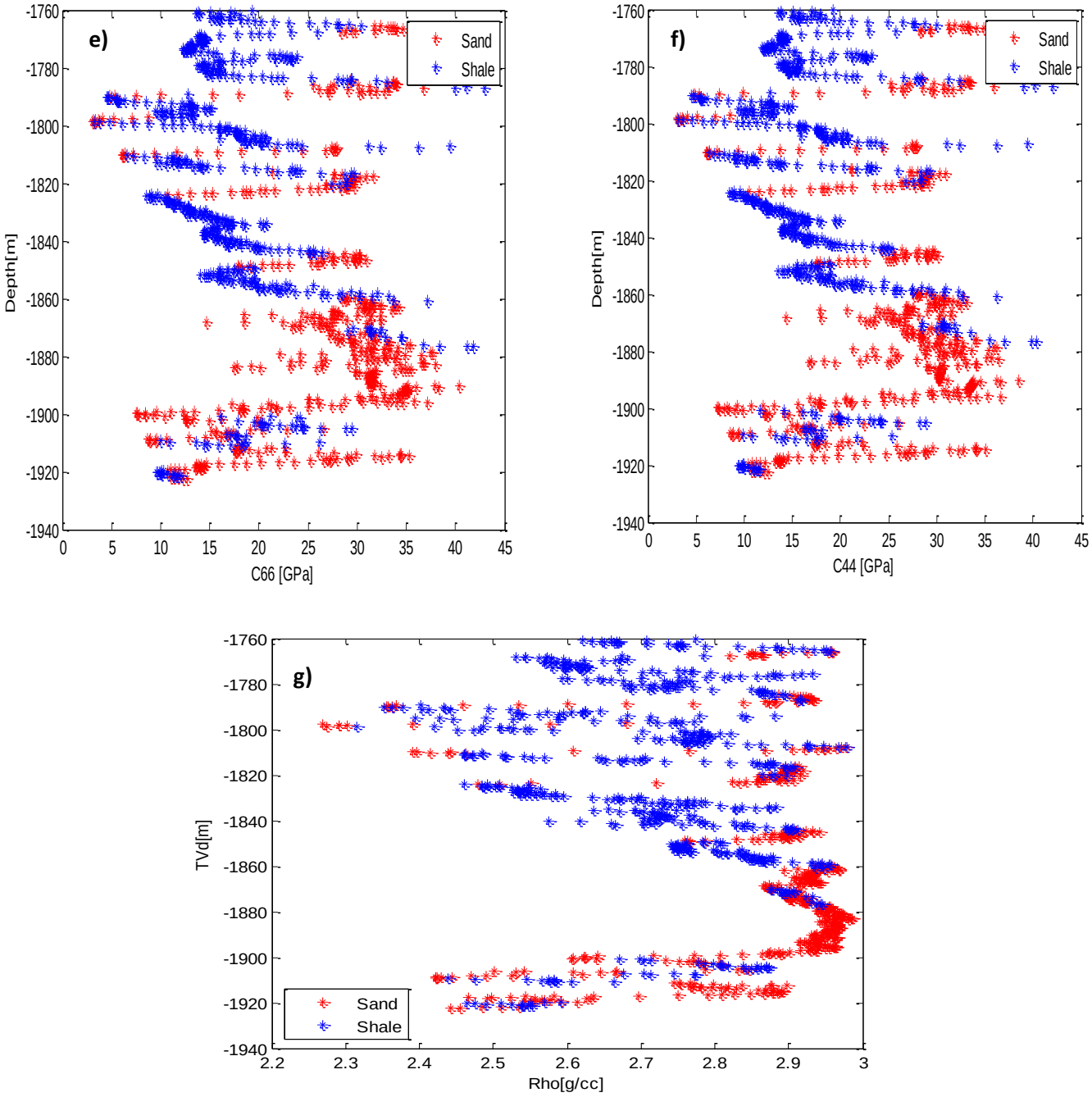

Figure 19. Intercalation of sand-shale with depth. (a) Model of the stiffness c_{11} with depth. (b) Model of the stiffness c_{12} with depth. (c) Model of the stiffness c_{13} with depth. (d) Model of the stiffness c_{33} with depth. (e) Model of stiffness c_{66} with depth. (f) model of stiffness c_{44} with depth. (g) Model of density with depth.

From fig. 19 a, there is a huge shale deposit at the depth of 1760 m – 1785 m with few sand sandwiched between the shale deposit. The shale has low stiffness which can be attributed to the fact that during deposition, shale has a high porosity of 80% - 90%. Also the stiffness of shale is a bit high at a depth of 1875 m – 1880 m. This may be due to onset of cementation. At the depth 1880 m – 1900 m, there is also a huge deposit of sand with high stiffness, more compacted, and less porous etc. This might be clean sand and can be a reservoir rock. On the other hand, the stiffness c_{33} also exhibits the same behavior. Both c_{11} and c_{33} are very high at a depth range of 1880 m – 1900 m. Their stiffness range between [80 – 88] GPa. Shale is also well pronounced at a depth of 1825 m -1860 m and 1760 m -1780 m with thin sand of few meters sandwiched between them. From fig. 19 c, there is a thick shale deposit at a depth 1760 m – 1860 m with thin sand sandwiched between the shale at the following depth; 1765 m – 1770 m, 1782 m – 1788 m, 1790 m – 1795 m, 1810 m – 1820 m and 1848 m – 1852 m. The shale has low stiffness, high porosity, loose sediments etc. In addition, the shale is more compact at the depth 1830 m – 1840 m. This is because, as we move deeper into the subsurface, sediments begin to accumulate and overburden increases, resulting in high compaction. Also at the depth 1865 m – 1920 m, there is a huge deposit of sand with thin shale sandwiched between them. The sand stiffness is high, thus it falls within [20 – 60] GPa. It is also more compact within the depth 1880 m – 1900 m and less compact at 1900 m – 1920 m. c_{13} also demonstrated the same behavior with depth. At a depth range of 1860 m – 1920 m, there is very thick sand with few shale sandwiched between the sand. The stiffnesses vary from [10 – 58] GPa. On the other hand, at a depth range of 1760 m – 1860 m there is a high concentration of shale with minute sand sandwiched between them. c_{66} and c_{44} also have the same pattern. Shale is most pronounced at the depth of 1760 m – 1780 m and 1825 m – 1845 m, while sand is most pronounced at a depth range of 1860 m -1900m. On the average, the shale has low stiffness as compared to the sand. From fig. 19 g, the sand is denser at a depth range 1875 m – 1900 m, while shale is less dense at a depth range of 1760 m – 1800 m, even though there are thin sand sandwiched between the shale, but the most predominant within the

depth 1760 m – 1880 m is the shale. The sand is also more pronounced within 1880 m – 1900 m. Its density is also very high. It falls within 2.9 g/cc – 3.0 g/cc.

VTI-VTI and Net to Gross Analysis

Figure 20. Models of effective properties versus net to gross.

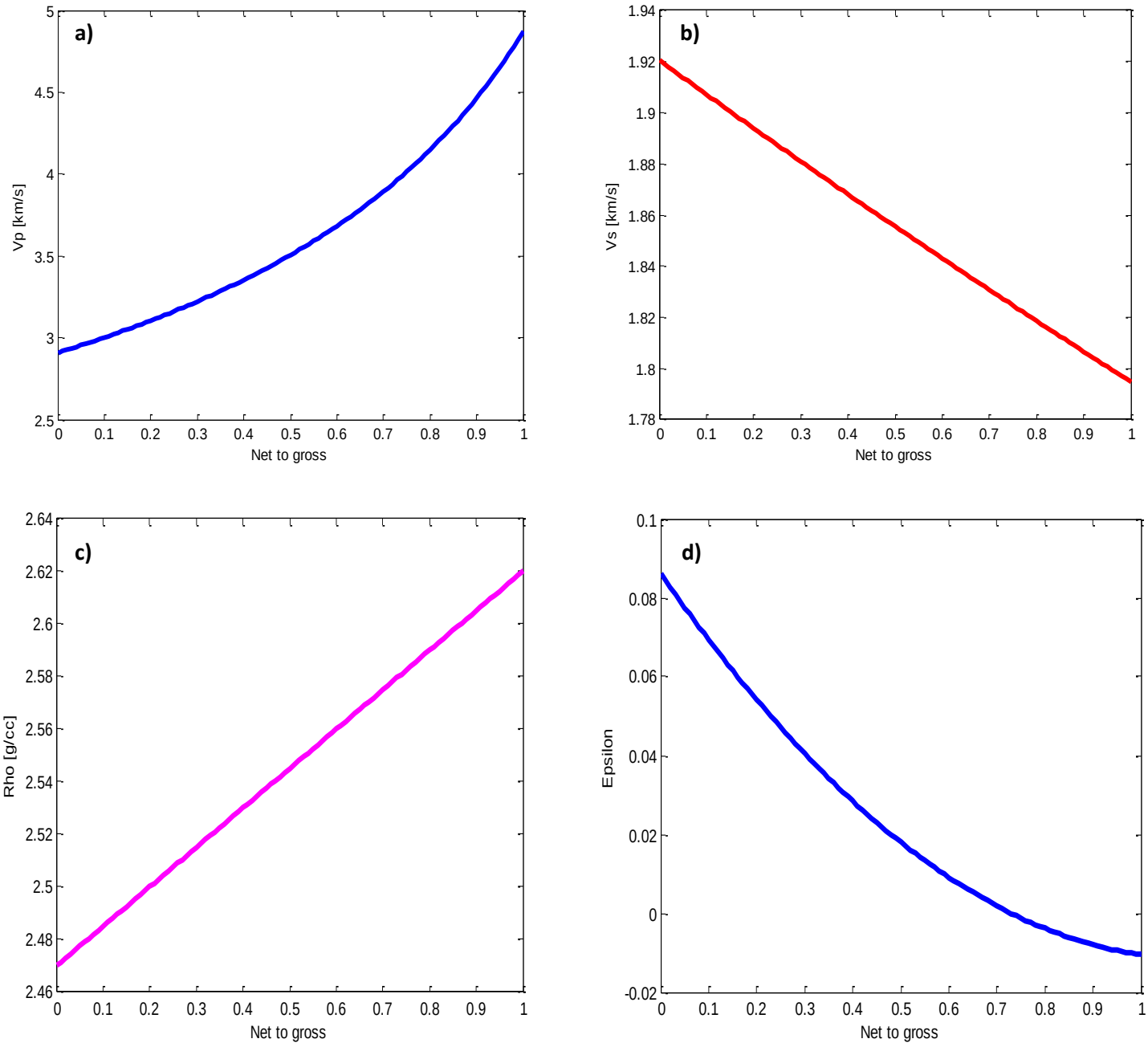

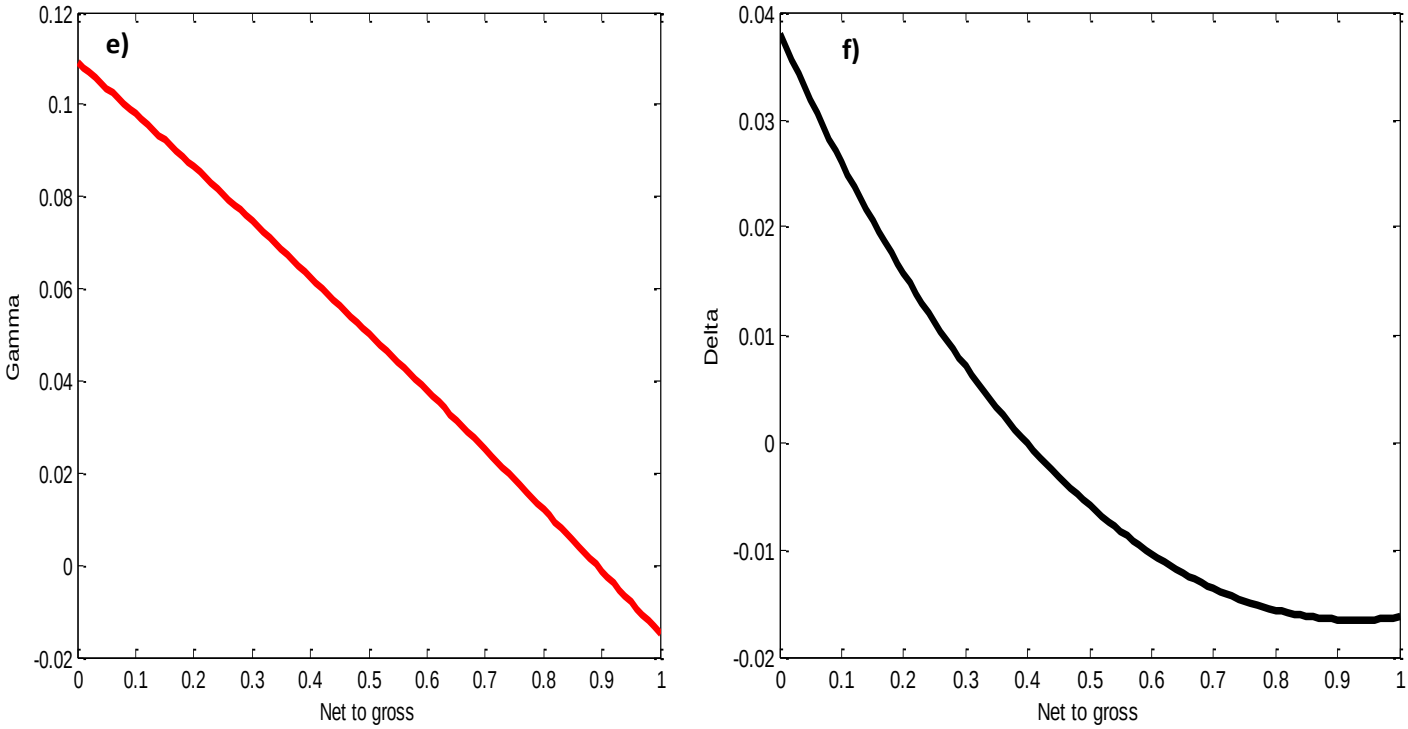

From fig. 20 a, there is an exponential increase in v_p as net to gross (N/G) increases. When net to gross is 0, v_p is 2.9 km/s and when net to gross is 1, v_p is 4.8 km/s. It indicates that v_p is high in pure sand and low in pure shale in this model. It also shows that giving equal volume of sand-shale intercalation and shale, the v_p in the sand-shale intercalation will be higher than that of the shale. This is because the sand – shale intercalation might have more porosity than the pure shale, and as a result fluid saturation in the sand – shale intercalation will be high which gives high v_p. When net to gross is 0, the shale has a v_p of 2.9 km/s which is far less than that of the sand with net to gross of 1. This shows that the shale is more compact, have high rock stiffness and low porosity. When net to gross started increasing from 0 to 0.1, v_p also increases, which indicates that the shale is becoming porous, less compacted and there is an onset of fluid.

From fig. 20 b, there is a gradual decrease in v_s as net to gross increases. This shows that v_s decreases with fluid saturation. When net to gross begins to increase, more

sand enters the formation and since sand is permeable, more fluid enters the formation and there is reduction in v_s. When net to gross is 0, v_s is 1.92 km/s which gives an indication of shale, while net to gross of 1 gives v_s of 1.795 km/s which indicates sand.

In model (c), the density increases with net to gross. This is because as net to gross increases more sand enters the formation. Therefore the stiffness becomes high and for that matter the density increases. Thus higher net to gross gives higher density and vice versa. When the net to gross is 0, the shale density is 2.47 g/cc and when net to gross is 1 the sand density is 2.62 g/cc.

From (d), there is an exponential decrease in anisotropic parameter epsilon as net to gross increases. When net to gross is 0, anisotropic parameter epsilon is 0.084, while net to gross of 1 gives epsilon -0.01. This shows that when we have more sand than shale in a formation, it affects the anisotropic value. When epsilon is 0.06, net to gross is 0.2 and when epsilon is 0.02, net to gross is 0.45. This gives a clear indication that the anisotropic parameter epsilon is high in shale than in sand.

Looking at model (e), there is a gentle decrease in anisotropic parameter gamma as net to gross increases. Net to gross of 0 corresponds to 0.11 anisotropic parameter gamma. On the other hand, net to gross of 1 corresponds to -0.015 anisotropic parameter gamma. From the model, it shows that shale is highly anisotropic, simply because it is fissile and laminated. Thus the rock readily splits into thin pieces along the lamination.

From (f), the anisotropic parameter delta decreases exponentially with increasing net to gross. Net to gross of 1 corresponds to -0017 delta, while net to gross of 0 corresponds to 0.038 delta. It also emphasize that shale is highly anisotropic than sand. Among the three anisotropic parameters, it follows that delta >gamma>epsilon.

VTI-HTI and Net to Gross Analysis

Fig 21. Models of effective properties versus net to gross.

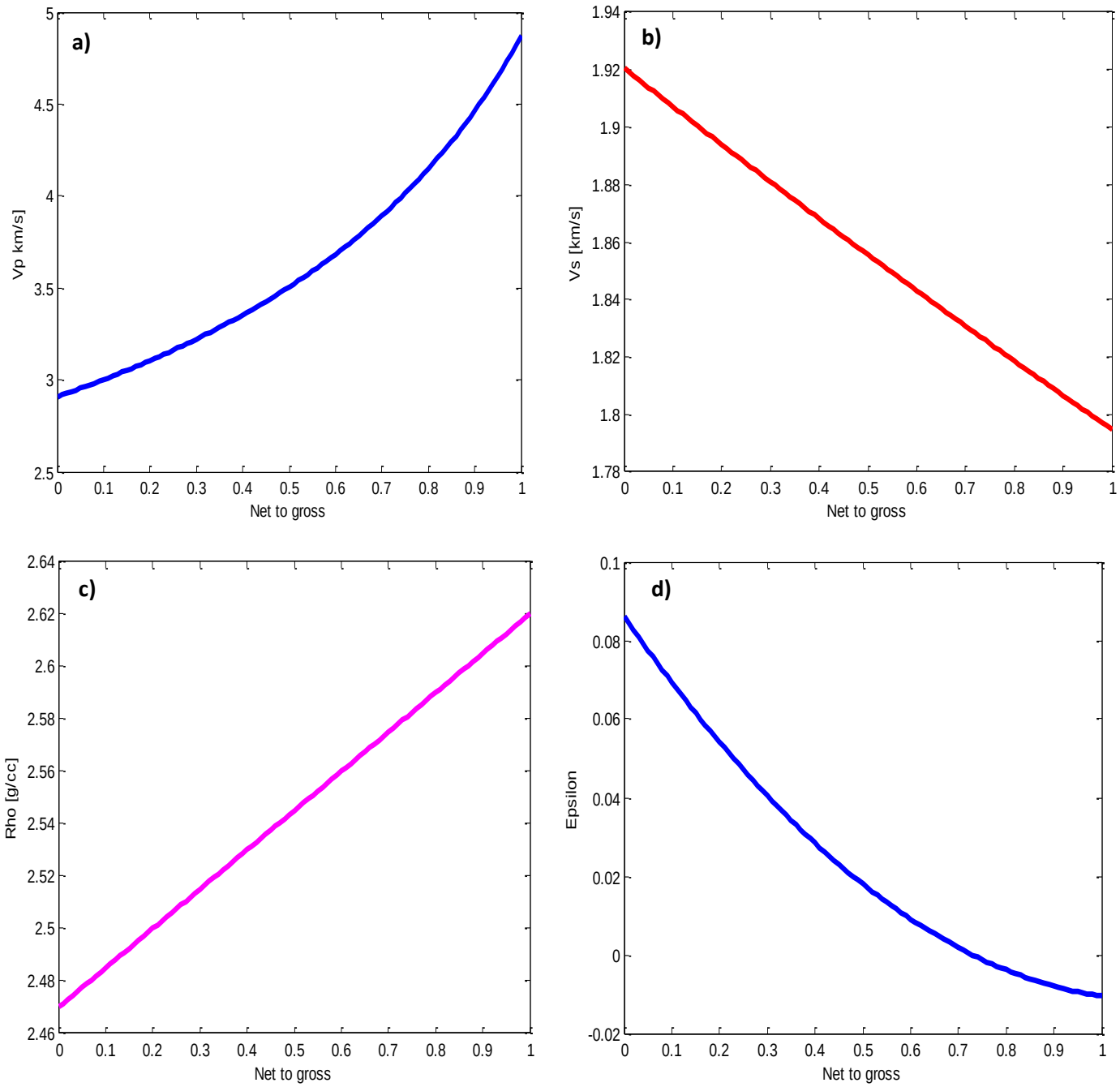

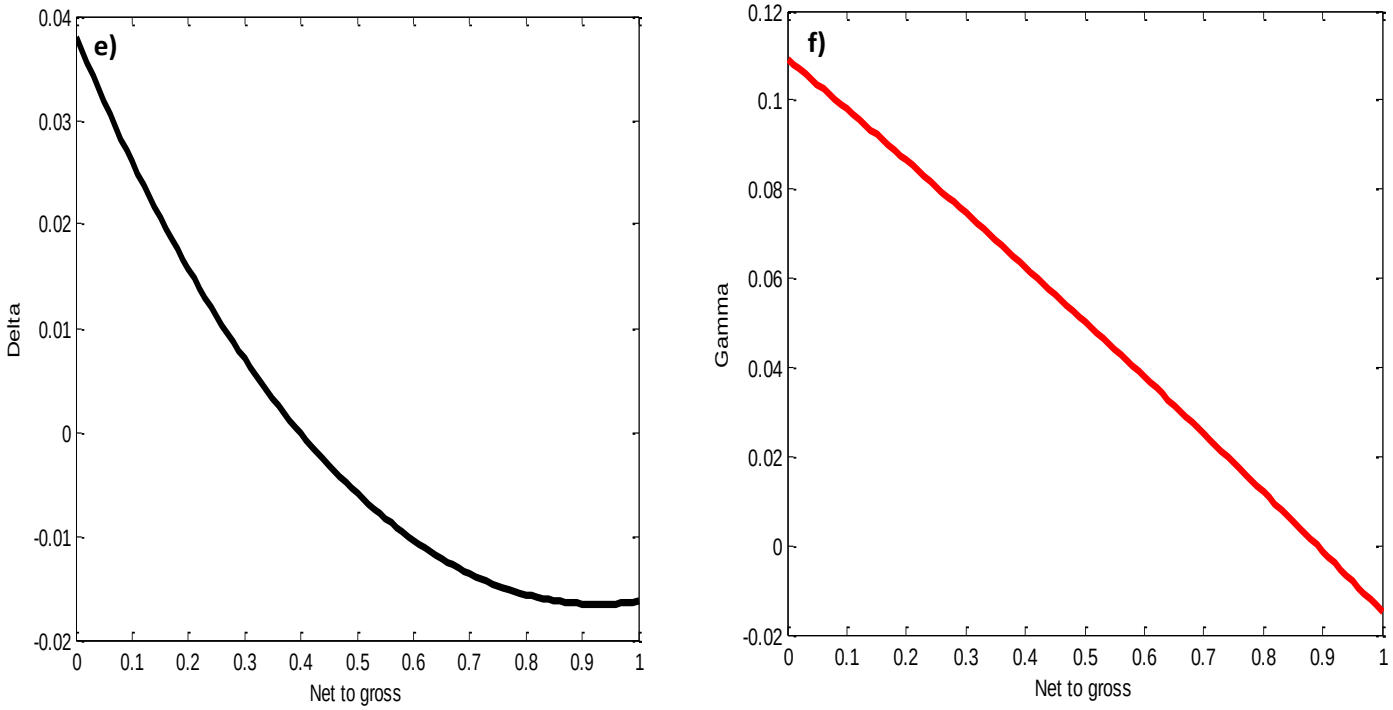

From fig. 21 a, there is an exponential increase in v_p as net to gross (N/G) increases. When v_p is 2.9 km/s, net to gross is 0, and when v_p is 4.8 km/s, net to gross is 1. It indicates that v_p is high in pure sand and low in pure shale in this case. It also shows that giving equal volume of shale and sand-shale intercalation, the v_p in the sand-shale intercalation will be higher than that of the shale. This is because the sand – shale intercalation might have more porosity than the pure shale, and as a result fluid saturation in the sand – shale intercalation will be high which gives high v_p. When net to gross is 0, the shale has a v_p of 2.9 km/s which is far less than that of the sand with net to gross of 1. This shows that the shale has high rock stiffness, more compact and low porosity. When net to gross started increasing from 0 to 0.1, v_p also increases, which indicates that the shale is becoming less compacted, porous and there is an influx of fluid.

From fig. 21 b, there is a gradual decrease in v_s as net to gross increases. This indicates that v_s decreases with fluid saturation. When net to gross begins to increase,

more sand enters the formation and since sand is permeable, more fluids enter the formation and there is reduction in v_s. When net to gross is 0, v_s is 1.92 km/s which gives an indication of shale, while net to gross of 1 gives v_s of 1.795 km/s which indicates sand.

In fig. 21 c, the density increases with net to gross. This is because as net to gross increases more sand enters the formation. Therefore the stiffness becomes high and for that matter the density increases. Thus higher net to gross gives higher density and vice versa. The shale density is 2.47 g/cc when net to gross is 0, and the sand density is 2.62 g/cc when net to gross is one.

From fig. 21 d, there is an exponential decrease in anisotropic parameter epsilon as net to gross increases. When net to gross is 0, anisotropic parameter epsilon is 0.084, while net to gross of 1 gives epsilon -0.01. This shows that when we have more sand than shale in a formation, it affects the anisotropic value. Several anisotropic values attest to the fact. When epsilon is 0.06, net to gross is 0.2, when epsilon is 0.04, net to gross is 0.35 and when epsilon is 0.02, net to gross is 0.45. This gives a clear indication that anisotropic parameter epsilon is high in the shale than in the sand model.

From (e), the anisotropic parameter delta decreases exponentially with increasing net to gross. Net to gross of 1 corresponds to -0017 delta, while net to gross of 0 corresponds to 0.038 delta. It also emphasize that shale is highly anisotropic than sand.

Looking at model (f), there is a gentle decrease in anisotropic parameter gamma as net to gross increases. Net to gross of 0 corresponds to 0.11 anisotropic parameter gamma. In addition, net to gross of 1 corresponds to -0.015 anisotropic parameter gamma. From the model, it shows that shale is highly anisotropic, simply because it is fissile and laminated. Thus the rock readily splits into thin pieces along the lamination. Among the three anisotropic parameters it follows that delta>gamma>epsilon.

Comparison between VTI – VTI and VTI – HTI

From fig. 21, I could see that the pattern of the models is similar to that of the VTI – VTI models (fig 20). The effective properties versus net to gross in both cases gave the

same results. Therefore, I can conclude that, there is no difference between the VTI – VTI test and the VTI – HTI test.

VTI-TTI 45° and Net to Gross Analysis

Fig. 22 Models of effective properties versus net to gross.

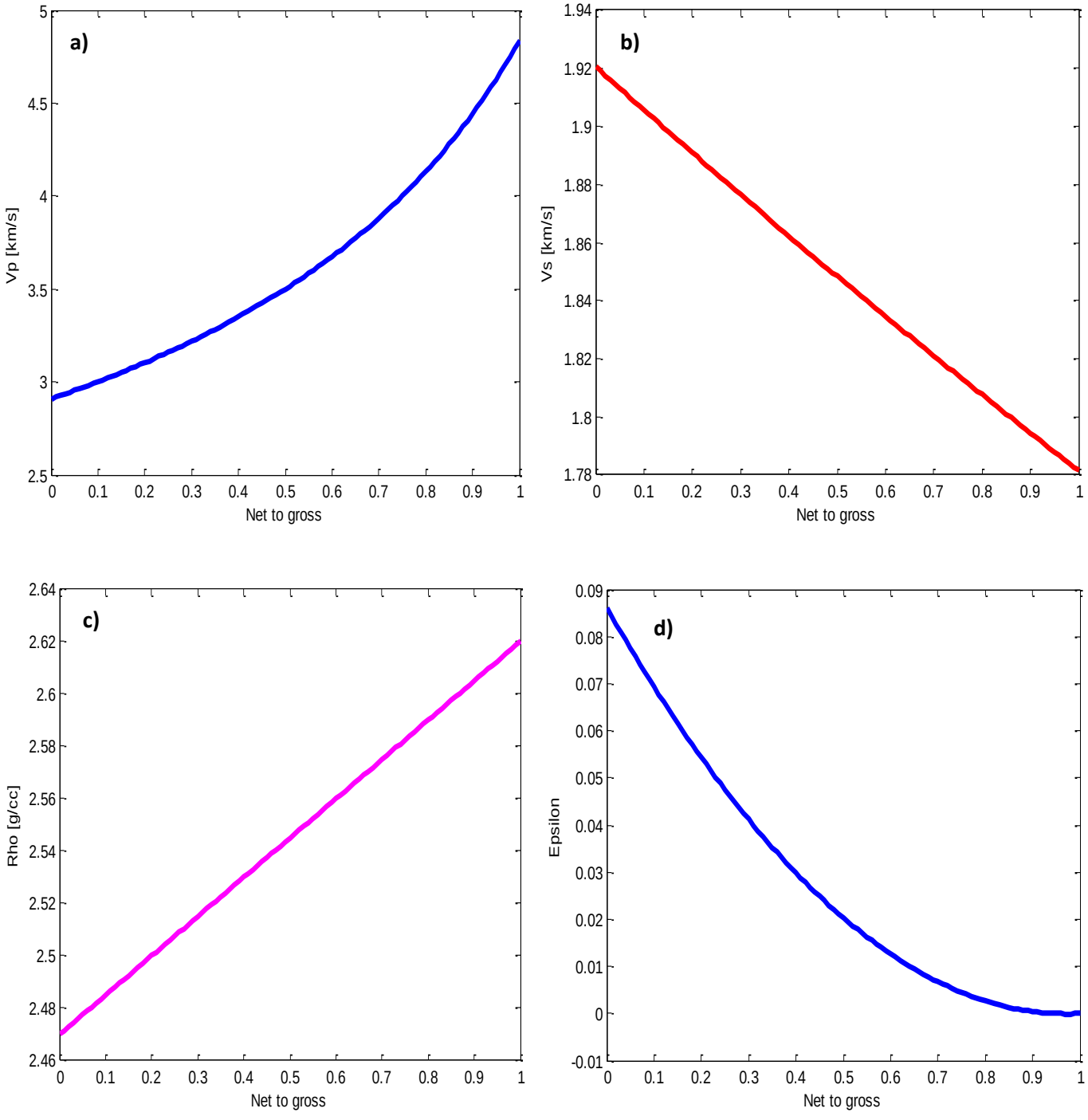

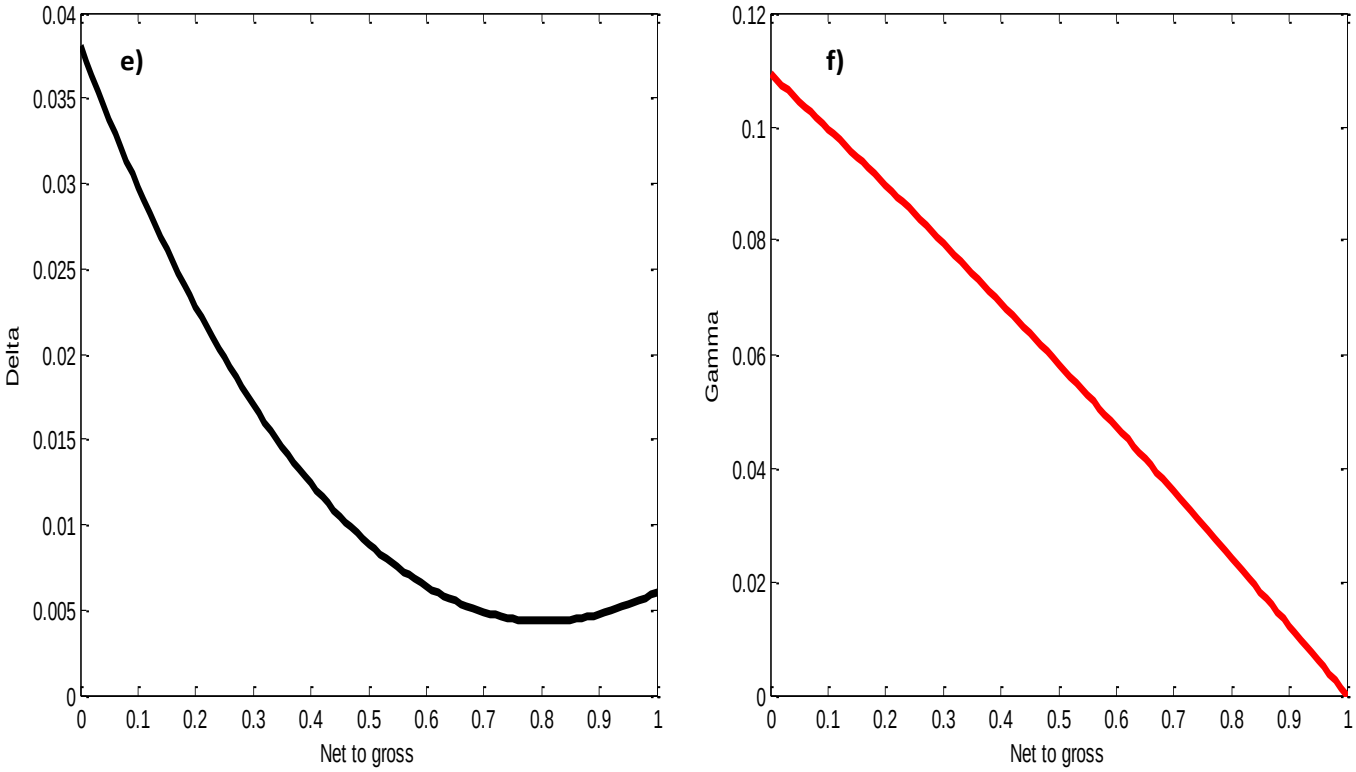

From fig. 22 a, there is an exponential increase in v_p as net to gross (N/G) increases. When v_p is 4.8 km/s, net to gross is 1, and when v_p is 2.9 km/s, net to gross is 0. It indicates that v_p is high in sand and low in shale in this case. It also shows that we might have high v_p in heterogeneous formation and low v_p in homogeneous formation and vice versa. Therefore giving equal volume of shale and sand-shale intercalation, the v_p in the sand-shale intercalation will be higher than that of the shale according to the model. This is because the sand – shale intercalation might have more porosity, high stiffness etc than the pure shale, and as a result fluid saturation in the sand – shale intercalation will be high which gives high v_p. When net to gross is 0, the shale has a v_p

of 2.9 km/s which is far less than that of the sand with net to gross of 1. This shows that the shale has low rock stiffness, less compacted and low porosity.

From fig. 22 b, there is a gradual decrease in v_s as net to gross increases. It started decreasing from 1.92 km/s to 1.782 km/s and its counterpart, thus net to gross also started increasing from 0 to 1. Therefore when sand in a formation begins to accumulate, more fluids enter the formation and as a result v_s decreases with fluid saturation. This is so, because v_s is not sensitive to fluids.

In fig. 22 c, the density increases with net to gross. The density of 2.47 g/cc has net to gross of 0. When the density started increasing net to gross also started rising. This is because as net to gross increases more sand enters the formation. Therefore the stiffness becomes high and for that matter the density increases. Thus higher net to gross gives higher density and vice versa. This can be seen in pure shale and pure sand. Empirically, the density of sand is higher than the density of shale.

From model 22 d, the anisotropic parameter epsilon, ε decreases exponentially with increasing net to gross. When net to gross is 0, epsilon, ε is 0.086, while net to gross of 1 gives 0 anisotropic parameter epsilon, ε. This shows that when we have pure shale which is transverse isotropy with tilted symmetry axis, the anisotropy value epsilon, ε obtained in that formation is very high. In the same way when we have pure sand with tilted symmetry axis, the anisotropy value is very low.

In fig 22 e, the anisotropic parameter delta, δ started decreasing exponentially from 0.038 to 0.005, while net to gross started increasing from 0 to 0.75. Anisotropic parameter delta, δ started increasing again from 0.005 to 0.006 while net to gross continues to increase. Therefore anisotropic parameter delta, δ varies in tilted transverse isotropy media. The variation mainly depends on the net to gross.

Looking at fig. 22 f, anisotropic parameter gamma, γ decreases with increasing net to gross. When net to gross is 1, the anisotropic parameter gamma, γ is 0 and when net to gross is 0, the anisotropic parameter gamma, γ is 0.11. This connotes that when we

have pure shale which is transverse isotropy with tilted symmetry axis, the anisotropy value gamma, γ obtained in that formation is very high. In the same way when we have pure sand with tilted symmetry axis, the anisotropy value is very low.

Comparison between VTI - TTI45° and VTI – VTI / VTI – HTI

From the models, I could see that the effective property v_p versus net to gross is the same for all the three symmetries. On the other hand, the effective property v_s of the VTI - TTI45° model differs slightly from the VTI – VTI and VTI – HTI models. Even though , they all decrease with increasing net to gross, the v_s against net to gross in the VTI - TTI45° model decreases faster than that of the VTI – VTI and VTI – HTI model. When net to gross is 1 in the VTI - TTI45° model, its v_s is 1.78 km/s while net to gross of 1 in the other models gives 1.795 km/s. The density models are also the same irrespective of the angle. In addition, the anisotropic parameters in the VTI - TTI45° model differs a bit from that of VTI – VTI and VTI – HTI. Anisotropic parameter epsilon, ε decreases exponentially with increasing net to gross. Net to gross of 1 gives epsilon, 0 in the VTI - TTI45° model, while net to gross of 1 gives epsilon, -0.01 in the case of the VTI – VTI and VTI – HTI. Therefore I can conclude that the anisotropic parameter, ε decreases slowly in the VTI - TTI45° model than in the VTI – VTI and VTI – HTI models. The situation looks different for delta, δ in the VTI - TTI45° model. The parameter decreases with increasing net to gross to some point and begin to increase with net to gross while that of the VTI – VTI and VTI – HTI models decrease with increasing net to gross. The behavior of gamma in the VTI - TTI45° model and that of the VTI – VTI and VTI – HTI models are almost the same. The only difference is that the VTI - TTI45° decreases slowly as compared with the VTI – VTI and VTI – HTI models. The anisotropic parameter gamma, γ of 0 is equivalent to net to gross of 1in the VTI - TTI45° model while gamma of 0 is equivalent to 0.9 net to gross in the other models. The values attest to the fact that gamma decreases slowly in the VTI - TTI45° than the VTI – VTI and VTI – HTI models.

Effective properties versus tilt in sand

Fig 23. Models of effective properties versus tilt in sand.

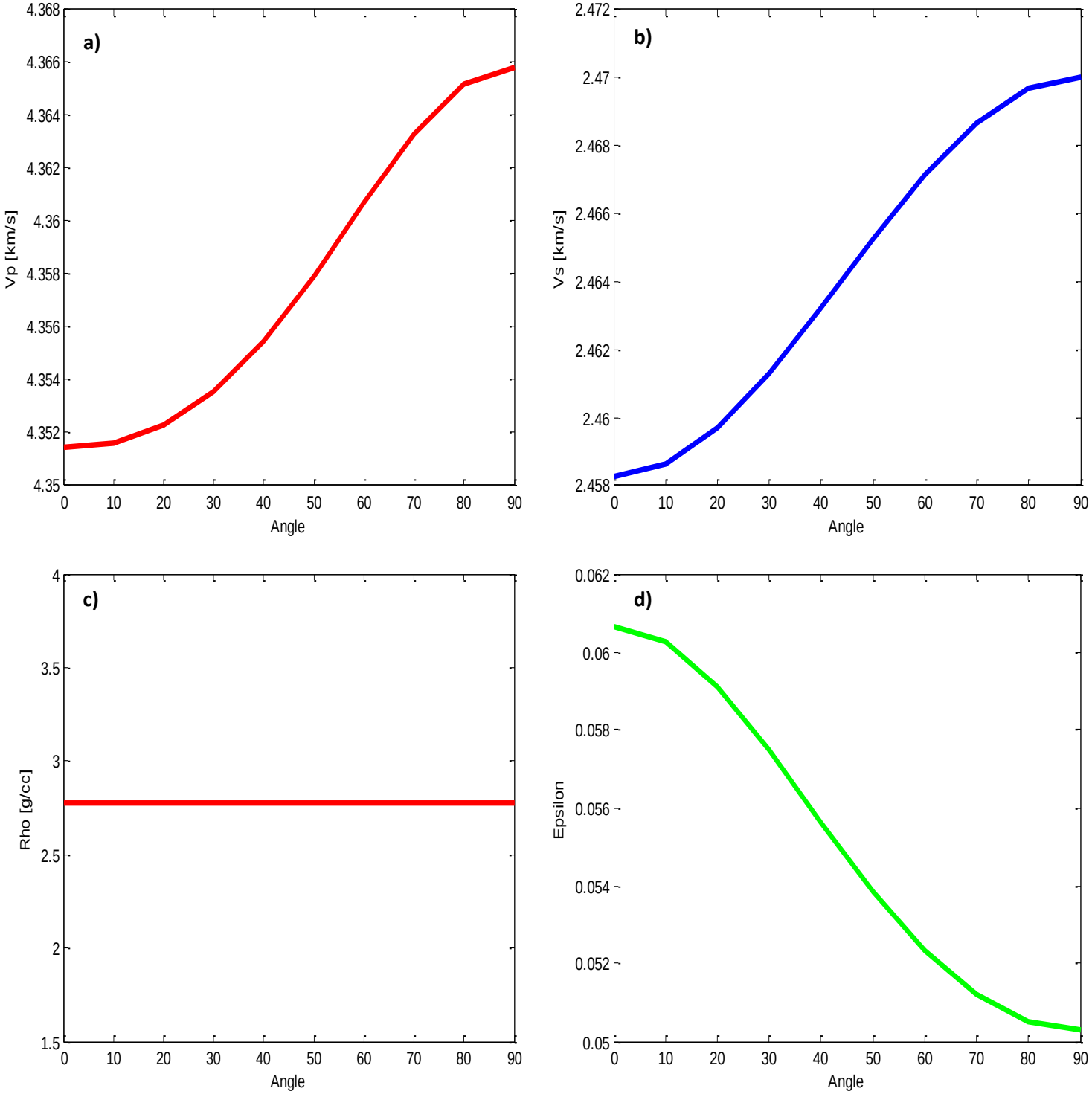

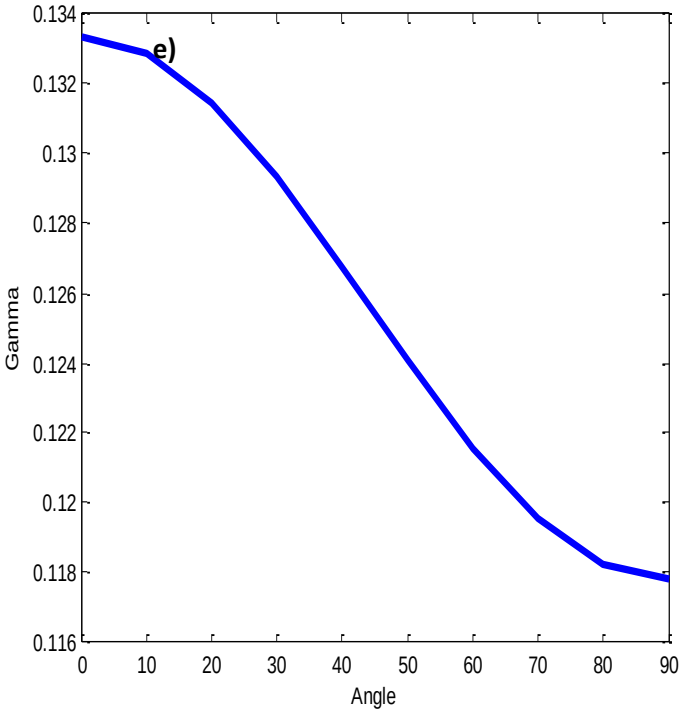

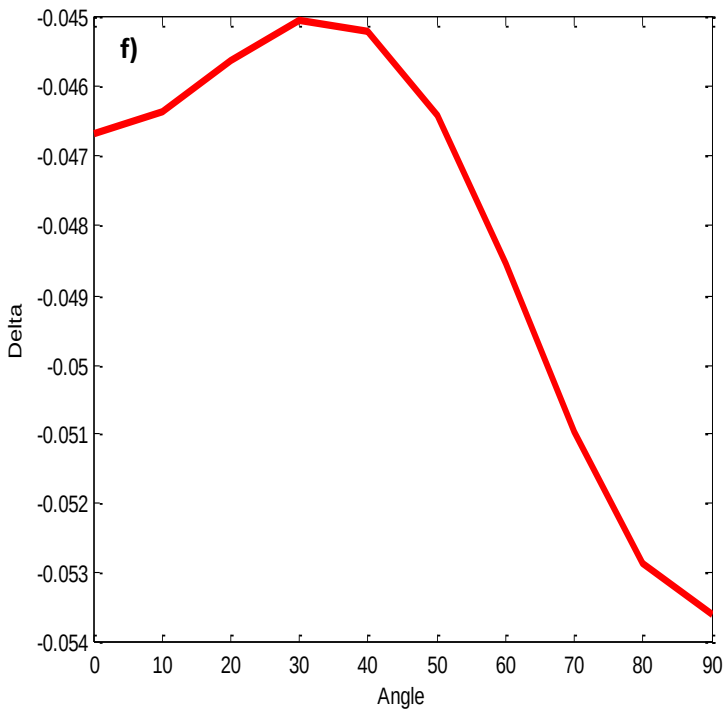

From fig. 23 a, effective property, v_p increases with angle. It started increasing steadily from 0° to 10°, then rose quickly from 10° to 80° and inclined in a gentle form from 80° to 90°. In a nutshell, v_p increases with tilt in sand. The same behavior is observed in fig. 23 b, where v_s increases steadily from 0° to 10° and rises quickly from 10° to 80°. It further increases from 80° to 90°. So I can infer that effective properties v_p and v_s increase with tilt angle in a homogeneous formation. The density remains constant with angle throughout the formation since the whole formation is considered as sand.

The patterns of the anisotropic parameters with tilt are different. From 23 d, anisotropic parameter epsilon, ε decreases with increasing angle. It started decreasing gently from 0.0607 to 0.0602 at an angle of 10°. It then reduces abruptly from 0.062 at 10° to 0.0504 at 80°, until coming to rest at 90°. The anisotropic parameter gamma, γ also exhibits the same behavior. It started decreasing from 0.1335 to 0.133 while tilt angle was increasing. It then declined quickly from 0.133 to 0.118 while tilt angle was increasing from 10° to 80°. It further declined from 0.118 to 0.1178 with the angle

increasing from 80° to 90°. But the situation looks different for anisotropic parameter delta, δ. Delta, δ started increasing with increasing angle up to 30°. It then began to decrease from 30° to 40° and declined further from 40° to 50°. It then declined abruptly from 40° to 80° and finally to 90°.

Comparison between effective properties versus tilt in sand and VTI –VTI/ VTI - HTI

Effective property, v_p increases with tilt in sand, and also increases with net to gross. v_s also increases with tilt in sand while it decreases with net to gross. Anisotropic parameter epsilon, ε decreases with tilt in sand and it also decreases with net to gross in the case of VTI – VTI and VTI – HTI. In addition, anisotropic parameter gamma, γ decreases with tilt in sand while it also decreases with net to gross. Delta, δ increases with tilt in sand up to 30° and decreases gradually to 90° while it decreases with net to gross in the case of VTI – VTI and VTI – HTI models.

Comparison between effective properties versus tilt in sand and VTI – TTI 45°

Effective property, v_p increases with tilt in sand, and increases with net to gross. Moreover, v_s increases with tilt in sand while it decreases linearly with net to gross. The anisotropic parameter, ε decreases with tilt in sand while it decreases exponentially with net to gross. The anisotropic parameter γ also decreases with increasing tilt in sand while it decreases exponentially with increasing net to gross. Finally, delta, δ increases from -0.0468 to -0.045 with tilt angle increasing from 0° to 30°. It then started decreasing with increasing tilt angle from 30° to 90°. On the other hand, delta decreases exponentially with increasing net to gross up to 0.75, and started increasing with net to gross up to 1.

CHAPTER FIVE

5.0 Conclusions

The main purpose of the thesis is to upscale real well log data using analytical equations presented by Backus (1962) and Schoenberg and Muir (1989). With regard to the upscaling, well log data from the North Sea is geologically analyzed with wave velocities (v_p, v_s), density and anisotropic parameters (epsilon, delta and gamma) in the form of transverse isotropy with vertical symmetry axis (VTI), horizontal symmetry axis (HTI) and tilted symmetry axis (TTI). Secondary properties such as v_p / v_s ratio and acoustic impedance are analyzed to discriminate between sand and shale.

In the first experiment (VTI-VTI test), the effective properties and anisotropic parameters compose of a mixture of two selected points representing sand and shale is analyzed to find the effect on net to gross using Backus (1962) averaging. Increasing net to gross increases P- wave velocity (v_p) and decreasing net to gross increases S- wave velocity (v_s). The decrease in net to gross can be misinterpreted as a change in fluid type or saturation.

In the second experiment (VTI-HTI), the two points representing sand and shale are mixed and the net to gross is estimated. The P- wave velocity (v_p) increases with increasing net to gross and the S- wave velocity (v_s) decreases with increasing net to gross. The anisotropic parameters (epsilon, delta and gamma) compose of a mixture of sand and shale is decreasing with increasing net to gross. The increase in net to gross is as a result of increasing porosity and permeability.

In the third experiment (VTI-TTI 45°), the models show that P- wave velocity (v_p) increases with increasing net to gross and S- wave velocity (v_s) decreases with increasing net to gross. The anisotropic parameters comprising sand and shale decrease with increasing net to gross due to saturation effects.

The final experiment uses the whole Intrabasalt 2 formation as tilt angle in sand. The P-wave velocity (v_p) and the S- wave velocity (v_s) increase with tilt angle in sand and the anisotropic parameters of the same formation decrease with tilt angle in sand with the exception of delta, which increases up to 30° and then decreases with tilt angle till it reaches 90°. The anisotropic parameter delta varies depending on the angle of propagation.

References

Alan F. Baird, J. Michael Kendall and Doug A. Angus, 2012, Frequency dependent seismic anisotropy due to fractures: Fluid flow versus scattering, university of Bristol, school of Earth Sciences, Bristol, UK and university of Leeds, school of Earth and Environment, Leeds, UK.

Anderson, D. L., 1961, Elastic wave propagation in layered anisotropic media: geophysics. Research, **66**, 2953 – 2964.

Andy Nowacki, James Wooky, J. Michael Kendall, 2011, New advances in using seismic anisotropy, mineral physics and geodynamics to understand deformation in the lowermost mantle. Journal of Geodynamics, **52**, 205 – 228.

Auld, B. A., 1990, Acoustic fields and waves in solids, 2nd Edition.

Backus, G. E., 1962, Long-wave elastic anisotropy produced by horizontal layering: Journal of Geophysics Research, **67**, 4427 – 4440.

Banik N. C., 1984, Velocity anisotropy of shales and depth estimation in the North Sea basin: Geophysics **49**, 1411 – 1419.

Berryman, J. G, Grechka, V. Y., and Berge, P. A, 1999, Analysis of Thomsen parameters for finely layered VTI media: Geophysical Prospecting, **47**, 959 – 978.

Carcione, J. M., 2007, Wave fields in Real Media: Theory and numerical simulation of wave propagation in anisotropic, anelastic, porous and electromagnetic media. Vol 38.

Carcione, J. M., Picott S, Cavallini, F and Santos, J. E., 2012, Numerical test of the Schoenberg – Muir theory, Geophysics, **77,** C25 – C35.

Crampin, S., 1985, Evidence of aligned cracks in the earth's crust: First Break **3**, 12-15.

Gaiser J, Chaveste A, Edrich M, Rebec T and Verm **R** 2011 Seismic anisotropy of the Marcellus shale: feasibility study for fracture characterization Recovery, CSPG CSEG CWLS Convention.

Gold, N., Shapiro, S. A., and Muller, T. M., 2000, An approach to Upscaling for seismic waves in statistically isotropic heterogeneous elastic media: Geophysics, **65**, 1837-1850.

Grechka, V., and M. Kachanov, 2006a, Seismic characterization of multiple fracture sets: Geophysics, **71**, 103 – 114.

Grechka, V., and M. Kachanov, 2006b, On effective elasticity of rocks with interacting and intersecting cracks: Geophysics, **71**, 103 – 114.

Helbig, K., 1958, Elastischen wellen in anisotropen medien: Geophysics, **67**, 256 – 288.

Hudson, J., 1981, wave speeds and attenuation of elastic waves in material containing cracks: Geophysical Journal of the Royal Astronomical Society, **64**, 133 – 150.

Hudson, J., E. Liu, and S. Crampin, 1997, The mean transmission properties of a fault with imperfect facial contact: Geophysical Journal International, **129**, 720 – 726.

Kendall, J. M., Q. J. Fisher, S. Covey Crump, J. Maddock, A. Carter, S. A. Hall, J. Wookey, S. L. A. Valke, M. Casey, G. Lloyd, and W. Ben Ismail, 2007, Seismic anisotropy as an indicator of reservoir quality in siliciclastic rocks: Geological Society, London, Special Publications, **292**, 123 – 136.

Liner, C. L., and Fei T. W., 2006, Layer-induced seismic anisotropy from full-wave sonic logs: theory, applications, and validation geophysics, **71**, d183-D190.

Landrø, M., 2012, seismic data acquisition and Imaging, NTNU.

Mavko G, Mukerji, T. and Dvorkin, J., 1998, The Rock physics handbook: Cambridge University Press.

Molotkov, L., and Khilo, A., 1985, Effective models for periodic anisotropic media: J. Sov. Math., **30**, 2445-2450.

Sams, M. S., and Williamson, P. R., 1994, Backus averaging, Scattering and drift: Geophysical prospecting, **42**, 541-564.

Sayers, C. M., 2005, Seismic anisotropy of shales: Geophysical prospecting, **53**, 667-676.

Sayers, C. M., 1994, P – wave propagation in weakly anisotropic media, Geophysics Journal International, **116**, 799 – 805.

Schoenberg M and Muir F., 1989, A calculus for finely layered anisotropic media, Geophysics, **54**, 581-589.

Schoenberg, M., 1985, An anisotropic model for a fractured, thinly layered elastic medium, 47th Annual Meeting of EAEG, Budapest.

Schoenberg, M., 1986, Wave propagation in an anisotropic medium with a system of aligned cracks, International Workshop on Seismic Anisotropy, Moscow.

Sheriff, Robert E. and Lloyd P. Geldart, 1995, Second Edition,Exploration Seismology page 38.

Sheriff, R. E., 2002, Encyclopedic Dictionary of Exploration Geophysics: Geophysical references series, Vol 13.

Shuang, Z., Robert E. K., and Patrick B., 2012, Micron to millimeter upscaling of shale rock properties Based on 3D imaging and modeling. Exxomobil Upstream Research Co., Houston, Tx, USA. VSG-Visualisation Sciences Group, Burlinton, MA, USA.

Stovas, A., and Arntsen, B., 2006, Vertical propagation of low – frequency waves in finely layered media: Geophysics, **71**, T87 – T94.

Thomsen, L., 2002, Understanding seismic anisotropy in exploration and exploitation: SEG Distinguished Intr. short course.

Thomsen, L., 1986, Weak elastic anisotropy: Geophysics, **51**, 1954 – 1966.

Thomsen, L., 1988, Reflection seismology over azimuthally anisotropic media: Geophysics, **53**, 304 – 313.

Thomson, W. T., 1950, Transmission of elastic waves through a stratified solid medium: Appl. Phys., **21**, 89 – 93.

Tsvankin, I., 1997, Reflection moveout and parameter estimation for horizontal transverse isotropy, Geophysics, **62**, 614-629.

Tsvankin, I., J. Gaiser, V. Grechka, M. van der Baan, and L. Thomsen, 2010, Seismic anisotropy in exploration and reservoir characterization: An overview: Geophysics, **75**, no.5, 75A15 – 75A29.

Valcke, S. L. A., M. Casey, G. E. Lloyd, J. M. Kendall, and Q. J. Fisher, 2006, Lattice preferred orientation and seismic anisotropy in sedimentary rocks: Geophysical Journal International, **166**, 652 – 666.

Vernik, L., and A. Nur, 1992, Ultrasonic velocity and anisotropy of hydrocarbon source rocks: geophysics, **57**, 727 – 735.

Webber, K.J., Van Geuns, L.C., 1990, Shell Intl. Petroleum Mij., Framework for constructing clastic Reservoir Simulation models, Journal of Petroleum Technology publisher: society of petroleum engineers, **42**

Younes et al, 2010, Sweet spotting the Haynesville-Bossier shale gas play, Northwestern Louisiana, an integrated study AAPG Hedberg Conference Austin Texas.

List of figures

Appendix

Matlab code

A.1. The script imports data containing depth, v_p, v_s, density, epsilon, delta, gamma, etc from datafile. A matlab algorithm was designed to carry out the Backus averaging and Schoenberg-Muir averaging.

```
load intrabasalt2.dat
%size(intrabasalt2)
N=1063
constant=2.3e7;
TVd=zeros(N,1);
Vp=zeros(N,1);
Vs=zeros(N,1);
Rho=zeros(N,1);
eps=zeros(N,1);
delta=zeros(N,1);
gamma=zeros(N,1);
ratio=zeros(N,1);
impedance=zeros(N,1);


TVd=intrabasalt2(:,1);
Vp=intrabasalt2(:,2);
Vs=intrabasalt2(:,3);
Rho=intrabasalt2(:,4);
eps=intrabasalt2(:,5);
delta=intrabasalt2(:,6);
gamma=intrabasalt2(:,7);
ratio=intrabasalt2(:,8);
impedance=intrabasalt2(:,9);
 for i=1:N
 C33(i)=Rho(i)*Vp(i)^2;
 C44(i)=Rho(i)*Vs(i)^2;
 C11(i)=C33(i)*(1+(2*eps(i)));
 C13(i)=sqrt((C33(i)-C44(i))*(C33(i)*(1+2*delta(i))-C44(i)))-C44(i);
 C66(i)=C44(i)*(1+(2*gamma(i)))
C12(i)=(C11(i)-(2*C66(i)))
 End
plot(impedance,ratio,'*')

 rationew=(constant)./impedance;
 hold on
 plot(impedance,rationew,'r');
```

```
 hold off

for i=[1:N]
if ratio(i)>rationew(i)
   flag(i)=1;
else
   flag(i)=0;
end
end
 flagone=find(flag==1);
 ratioup=ratio(flagone);
 impedanceup=impedance(flagone);
 flagzero=find(flag==0);
 ratiodown=ratio(flagzero);
 impedancedown=impedance(flagzero);
 figure
 plot(impedanceup,ratioup,'*r')
 hold on
 plot(impedancedown,ratiodown,'*')
 plot(impedance,rationew,'-m')
plot(Vp,TVd)
 plot(Vs,TVd,'r')
 plot(Rho,TVd,'m')
 plot(eps,TVd,'r')
 plot(delta,TVd,'c')
 plot(gamma,TVd,'g')
 plot(C11,TVd)
 plot(C13,TVd,'r')
 plot(C66,TVd,'m')
 plot(C44,TVd,'k')
 plot(C33,TVd,'g')
```

A 2.

```
clear all;
close all;

load intrabasalt3.dat
%size(intrabasalt3)
N=1063;
constant=2.3e7;
TVd=zeros(N,1);
Vp=zeros(N,1);
Vs=zeros(N,1);
Rho=zeros(N,1);
```

```
eps=zeros(N,1);
delta=zeros(N,1);
gamma=zeros(N,1);
ratio=zeros(N,1);
impedance=zeros(N,1);


TVd=intrabasalt3(:,1);
Vp=intrabasalt3(:,2);
Vs=intrabasalt3(:,3);
Rho=intrabasalt3(:,4);
eps=intrabasalt3(:,5);
delta=intrabasalt3(:,6);
gamma=intrabasalt3(:,7);
ratio=intrabasalt3(:,8);
impedance=intrabasalt3(:,9);
 for i=1:N
 C33(i)=Rho(i)*Vp(i)^2/1000000000;
 C44(i)=Rho(i)*Vs(i)^2/1000000000;
 C11(i)=C33(i)*(1+(2*eps(i)));
 C13(i)=sqrt((C33(i)-C44(i))*(C33(i)*(1+2*delta(i))-C44(i)))-C44(i);
 C66(i)=C44(i)*(1+(2*gamma(i)));
C12(i)=(C11(i)-(2*C66(i)));
 end



 plot(impedance,ratio,'*')

 rationew=(constant)./impedance;
 hold on
 plot(impedance,rationew,'r');
  hold off

 for i=[1:N]
 if ratio(i)>rationew(i)
    flag(i)=1;
 else
    flag(i)=0;
 end
 end


 flagone=find(flag==1);
 TVd_sand=TVd(flagone);
 C11_sand=C11(flagone);
```

```
plot(C11_sand,TVd_sand,'r*'),hold on

flagzero=find(flag==0);
TVd_shale=TVd(flagzero);
C11_shale=C11(flagzero);
plot(C11_shale,TVd_shale,'b*'),hold off
Xlabel('C11')
Ylabel('Depth[m]')
legend('Sand','Shale')
```

A 3.

VTI – VTI test

```
clear all;
close all;
load code2.dat
size(code2);
code2
C11=zeros(N,1);
C12=zeros(N,1);
C13=zeros(N,1);
C33=zeros(N,1);
C44=zeros(N,1);
C66=zeros(N,1);
Rho=zeros(N,1);

C11=code2(:,1);
C12=code2(:,2);
C13=code2(:,3);
C33=code2(:,4);
C44=code2(:,5);
C66=code2(:,6);
Rho=code2(:,7);
for i=1:101;
ng=(i-1)/100;
A1(i)=(C11(1)-((C13(1)^2)/C33(1)))*(ng)+((1-ng)*(C11(2)-((C13(2)^2)/C33(2))));
A2(i)=((C13(1)/C33(1))*(ng))+((1-ng)*(C13(2)/C33(2)));
A3(i)=((1/C33(1))*(ng))+((1/C33(2))*(1-ng));
A4(i)=((1/C44(1))*(ng))+((1/C44(2))*(1-ng));
A5(i)=((C66(1))*(ng))+((C66(2))*(1-ng));
Density(i)=(Rho(1)*(ng))+((Rho(2))*(1-ng));
```

```
C11ef(i)=A1(i)+((A2(i)^2)/A3(i));
C13ef(i)=A2(i)/A3(i);
C33ef(i)=1/A3(i);
C44ef(i)=1/A4(i);
C66ef(i)=A5(i);
Vpef(i)=sqrt(C33ef(i)/Density(i));
Vsef(i)=sqrt(C44ef(i)/Density(i));
epsef(i)=(C11ef(i)-C33ef(i))/(2*C33ef(i));
deltaef(i)=((C13ef(i)+C44ef(i))^2-(C33ef(i)-C44ef(i))^2)/(2*C33ef(i)*(C33ef(i)-C44ef(i)));
gammaef(i)=(C66ef(i)-C44ef(i))/(2*C44ef(i));
end
 ng=[0:0.01:1];
 plot(ng,gammaef,'m')
 ylabel('gamma')
xlabel('Net to gross')
figure
 plot(ng,deltaef)
title('Delta')
figure
 plot(ng,epsef)
title('Gamma')
plot(ng,C11ef)
plot(ng,C13ef)
plot(ng,C33ef)
plot(ng,C44ef)
plot(ng,Vsef)
```

A 4.

VTI – HTI test

```
clear all;
close all;
load final2.dat
size(final2);
Net=final2(:,1);
Vp=final2(:,2);
Vs=final2(:,3);
Rho=final2(:,4);
eps=final2(:,5);
```

```
delta=final2(:,6);
gamma=final2(:,7);
plot(Net,Vp);
plot(Net,Vs,'r');
 plot(Net,Rho,'m');
 plot(Net,eps);
 plot(Net,delta,'k');
 plot(Net,gamma,'r');
```

A 5.

VTI – TTI 45 degree test

```
clear all;
close all;
load shoenberg45.dat
size(shoenberg45);
Net=shoenberg45(:,1);
Vp=shoenberg45(:,2);
Vs=shoenberg45(:,3);
Rho=shoenberg45(:,4);
eps=shoenberg45(:,5);
delta=shoenberg45(:,6);
gamma=shoenberg45(:,7);
plot(Net,Vp);
plot(Net,Vs,'r');
plot(Net,Rho,'m');
plot(Net,eps);
plot(Net,delta,'k');
plot(Net,gamma,'r');
```

A 6.

Effective properties versus tilt in sand

```
load intra.dat
size(intra);
angle=intra(:,1);
```

```
zero1=intra(:,2);
Vp=intra(:,3);
Vs=intra(:,4);
Rho=intra(:,5);
eps=intra(:,6);
del=intra(:,7);
gamma=intra(:,8);
zero2=intra(:,9);
plot(angle,eps,'g');
```